Advanced Optical Technologies

TYPE Review
PUBLISHED 11 April 2025
DOI 10.3389/aot.2025.1560084

Check for updates

OPEN ACCESS

EDITED BY
Régis Orobtchouk,
Institut National des Sciences Appliquées de Lyon (INSA Lyon), France

REVIEWED BY
Shuang Chang,
Vanderbilt University, United States
Idris Kabalci,
Uşak University, Türkiye

*CORRESPONDENCE
Nicola Montaut,
nicola.montaut@inrs.ca
Roberto Morandotti,
roberto.morandotti@inrs.ca

†PRESENT ADDRESS
Monika Monika,
Photonic Quantum Systems, Fraunhofer Institute for Applied Optics and Precision Engineering, Jena, Germany
Farzam Nosrati,
IMDEA Networks Institute, Madrid, Spain

RECEIVED 13 January 2025
ACCEPTED 18 March 2025
PUBLISHED 11 April 2025

CITATION
Montaut N, George A, Monika M, Nosrati F, Yu H, Sciara S, Crockett B, Peschel U, Wang Z, Lo Franco R, Chemnitz M, Munro WJ, Moss DJ, Azaña J and Morandotti R (2025) Progress in integrated and fiber optics for time-bin based quantum information processing.
Adv. Opt. Technol. 14:1560084.
doi: 10.3389/aot.2025.1560084

Progress in integrated and fiber optics for time-bin based quantum information processing

Nicola Montaut[1]*, Agnes George[1], Monika Monika[1,2], Farzam Nosrati[1,3†], Hao Yu[1,4], Stefania Sciara[1], Benjamin Crockett[1], Ulf Peschel[2], Zhiming Wang[4], Rosario Lo Franco[3], Mario Chemnitz[1,5,6], William J. Munro[7,8], David J. Moss[9], José Azaña[1] and Roberto Morandotti[1]*

[1]Institut National de la Recherche Scientifique - Centre Énergie, Matériaux et Télécommunications (INRS-EMT), Varennes, QC, Canada, [2]Institute of Condensed Matter Theory and Optics, Friedrich-Schiller-University, Jena, Germany, [3]Dipartimento di Ingegneria, Università degli Studi di Palermo, Palermo, Italy, [4]Shimmer Center, Tianfu Jiangxi Laboratory, Chengdu, China, [5]Smart Photonics Department, Leibniz Institute of Photonic Technology, Jena, Germany, [6]Institute of Applied Optics and Biophysics, Abbe Center of Photonics, Friedrich-Schiller-University, Jena, Germany, [7]Okinawa Institute of Science and Technology Graduate University, Onna-son, Okinawa, Japan, [8]National Institute of Informatics, Tokyo, Japan, [9]Optical Sciences Centre, Swinburne University of Technology, Hawthorn, VIC, Australia

The development of integrated photonic systems, both on-chip and fiber-based, has transformed quantum photonics by replacing bulky, fragile free-space optical setups with compact, efficient, and robust circuits. Photonic platforms incorporating fiber-connected sources of correlated and entangled photon pairs offer practical advantages, such as operation at room temperature, efficient integration with telecom infrastructure, and compatibility with mature and efficient semiconductor fabrication processes for cost-effective and large-scale optical circuits. The stability and scalability of integrated quantum photonics platforms have facilitated the generation and processing of quantum information in the temporal domain within a single spatial mode. Time-bin encoded states, known for their robustness against decoherence and compatibility with existing fiber-optic infrastructure, have shown to be an efficient paradigm for advanced applications like quantum secure communication, information processing, spectroscopy, imaging, and sensing. This review examines recent advancements in fiber- and chip-based platforms for generating non-classical states and their applications as quantum state processors in the time domain. We discuss the generation of pulsed quantum frequency combs using microring resonators and intra-cavity mode-locked laser schemes, enabling co- and cross-polarized quantum photonic states. Additionally, the versatility of these resonator chips for entanglement generation is emphasized, including two- and multi-photon time-bin entangled schemes. We highlight the development of time-bin entanglement analyzers in fiber architectures, featuring ultrahigh stability and post-selection-free capabilities, which enable precise and efficient characterization of two- and higher-dimensional time-bin entanglement. We also review scalable on-chip schemes for quantum key distribution, demonstrating low quantum bit error rates and compatibility with higher-dimensional quantum communication protocols. Further, methods for enhancing temporal resolution in detection schemes, crucial for time-bin encoding, are presented, such as the time-stretch sampling technique using electro-optic modulation. These innovations, relying on readily available, telecom-based fiber-optic components, provide practical, scalable, and cost-effective solutions for advancing quantum photonic technologies. Looking forward, time-bin encoding is expected to play a pivotal role in the advancement of quantum repeaters, distributed quantum networks, and hybrid light-matter systems, advancing the realization of globally scalable quantum technologies.

KEYWORDS

time-bin encoding, higher-dimensional entanglement, time-bin analyzers, post-selection-free measurements, fiber and integrated photonics, synthetic photonic lattices, cluster states, quantum optical sampling scope

1 Introduction

There is a growing demand for practical and scalable architectures to deploy quantum photonic technologies (Moody et al., 2022) for applications such as quantum secure communication (Krenn et al., 2016a; Lu et al., 2019; Cozzolino et al., 2019; Kimble, 2008), metrology (Giovannetti et al., 2011; Matthews et al., 2016; Slussarenko et al., 2017), computing (Flamini et al., 2018; Arrazola et al., 2021; Harrow and Montanaro, 2017; Bromley et al., 2020; Knill et al., 2001), and sensing (Pirandola et al., 2018; Israel et al., 2014). The advent of integrated photonic platforms has opened the possibility for low-footprint, power-efficient, reliable, and stable solutions for quantum state preparation and processing (Bonneau et al., 2016; Caspani et al., 2017; Caspani et al., 2016; Pelucchi et al., 2021), while offering reduced propagation losses (Blumenthal, 2020) and improved scalability (Walmsley, 2015; Shadbolt et al., 2012; Jin et al., 2014). Losses present a significant challenge in quantum photonic devices, as they cannot be compensated through amplification like in classical systems. The no-cloning theorem (Wootters and Zurek, 1982) prohibits the deterministic amplification of quantum states, making it essential to minimize losses across all optical components. This is particularly crucial for applications such as quantum information processing (Varnava et al., 2008) and Bell inequality tests (Eberhard, 1993), which are inherently sensitive to losses. To address this, quantum photonic devices require low-loss interfaces that leverage the advantages of both fiber and integrated platforms, enabled by high chip-to-fiber coupling efficiencies (He et al., 2019; Son et al., 2018; Musiał et al., 2020; Elshaari et al., 2020). These efficiencies are achieved through meticulously engineered tapered waveguides (Kasaya et al., 1993; Noda et al., 1978; Alder et al., 2000) and grating couplers (Cheben et al., 2010; Cheben et al., 2015; Barwicz et al., 2015), which significantly enhance device throughput.

Integrated silicon-based platforms have demonstrated significant potential in enabling diverse on-chip quantum photonic functionalities, including spontaneous four-wave mixing for nonlinear frequency conversion (Liu et al., 2012; Li et al., 2016; Reimer et al., 2014; Roztocki et al., 2017; Reimer et al., 2015; Reimer et al., 2016; Kues et al., 2017; Reimer et al., 2019), low-loss waveguides for efficient photon routing (Wilmart et al., 2019; Wilmart et al., 2021; Wilmart et al., 2022; Ye et al., 2022; Frigg et al., 2019), and reconfigurable optical circuits for tailorable quantum states (Clementi et al., 2023; Taballione et al., 2021; Taballione et al., 2019). Leveraging the compatibility with complementary metal–oxide–semiconductor (CMOS) technologies, increasingly complex integrated photonics chips have been developed, incorporating on-chip tunable (reconfigurable) active elements for dynamic optical manipulations and optimized quantum state measurements (Shadbolt et al., 2012; Jin et al., 2014; Clementi et al., 2023; Taballione et al., 2021; Taballione et al., 2019; Metcalf et al., 2014). These advancements enable the miniaturization of table-top experiments into compact, chip-sized prototypes, paving the way for scalable quantum technologies.

Photonic schemes offer numerous advantages compared to other quantum systems based on, e.g., solid-state architectures such as superconducting qubits (Mooney et al., 2019), neutral atoms (Bernien et al., 2017; Henriet et al., 2020), and ion traps (Debnath et al., 2016; Niffenegger et al., 2020), which operates at cryogenic temperatures, while most photonic platforms rely on room temperature operation (Bourassa et al., 2021; Lu et al., 2021) for quantum state generation and processing. Photons, as carriers of information, are less prone to decoherence, allowing transmission over long distances, spanning hundreds (Yin et al., 2012; Krenn et al., 2016b; Boaron et al., 2018) to thousands (Yin et al., 2017; Liao et al., 2017) of kilometers. This makes them excellent candidates for satellite- (Yin et al., 2017; Liao et al., 2017) and fiber- (Boaron et al., 2018; Korzh et al., 2015; Ma et al., 2012) based quantum communication frameworks. Photons also exhibit several degrees of freedom (DoFs) such as polarization (Burlakov et al., 2001; Zhu et al., 2012; Chen et al., 2022), optical path (Rossi et al., 2009; Schaeff et al., 2012; Wang et al., 2018), orbital angular momentum (Mair et al., 2001; Jennewein et al., 2000), time (Reimer et al., 2016; Reimer et al., 2019; Brendel et al., 1999; Ali-Khan et al., 2007; Yu et al., 2024) and frequency (Kues et al., 2017; Imany et al., 2018; Olislager et al., 2010), all of which can be harnessed to generate diverse types of quantum states including single and correlated photon states (Reimer et al., 2014; Roztocki et al., 2017; Reimer et al., 2015), as well as complex photonic systems such as entangled and cluster states (Reimer et al., 2016; Kues et al., 2017; Reimer et al., 2019). Photonic DoFs further enable access to higher-dimensional quantum states–qudits–which yield several advantages compared to qubits in terms of increased information storage, processing capacity, and noise tolerance (Wang et al., 2020; Miller et al., 2018; Huang et al., 2022; Zhang et al., 2022), all of which improves as the photons' dimensionality (number of levels) is scaled up (Collins et al., 2002; Sciara et al., 2019). Furthermore, the complexity of qudit-based photonic schemes is significantly lower than their qubit-based counterparts, as the need for multi-qubit operations are replaced by parallel processing of information facilitated by the high dimensionality of qudits. Overall, the features associated with photonic qudits have shown to provide immediate advantages in enhancing the efficiency of quantum communication and greater accuracy in quantum computation schemes (Shor, 1994; Kitaev, 1995). Additionally, they enable reduced circuit depths–measured by the number of sequential gate operations–thereby optimizing quantum computation schemes (Chi et al., 2022).

Various parametric photonic sources have been engineered to generate qubit and qudit states via spontaneous parametric down-conversion (SPDC, a second-order nonlinear process (Harris et al., 1967; Magde and Mahr, 1967)) and spontaneous four-wave mixing (SFWM, a third-order nonlinear process (Sharping et al., 2001; Wang et al., 2001; Takesue and Inoue, 2004)). Both processes yield biphoton quantum states, namely signal and idler, when a nonlinear medium is exposed to a pump excitation field. This review focuses on photon sources based on dielectric and CMOS platforms implemented in waveguides and microring resonators (MRRs) which are capable of generating broadband quantum states in the telecom wavelength range, an optical regime characterized by minimal transmission losses in standard single-mode fibers. Waveguides yield a continuous spectra, whereas MRRs provide equally spaced frequency lines, forming a quantum frequency comb (QFC) (Pasquazi et al., 2018). These platforms can be engineered to operate in a single spatial mode compatible with standard fiber-optic components (Caspani et al., 2016), making them well-suited for practical, out-of-the-lab applications. They provide exciting opportunities for higher-dimensional quantum state generation by leveraging multiple time and frequency modes, addressing scalability and complexity challenges in quantum photonic technologies. These schemes also offer reliable means of processing light using commercially available devices and enable transmission over long distances via fiber-based and free-space architectures (Reimer et al., 2016; Kues et al., 2017; Ikuta and Takesue, 2018). Furthermore, MRR platforms enable the generation of nearly pure (single frequency mode) photonic states (Helt et al., 2010), a spectral response tailored through the quality factor of the resonator, providing fundamental resources for multi-source interference schemes, e.g., for quantum computation (Knill et al., 2001). This is unlike waveguide-based architectures, where pure states are typically generated via strong spectral filtering (Zeilinger et al., 1997), leading to a significant loss of photons, in turn lowering the efficiency. However, achieving truly pure biphoton states in MRRs requires the pump resonance quality factor to be lower than that of the biphoton states (Vernon et al., 2017), a condition that is unmet in conventional MRR designs (Helt et al., 2010; Silverstone et al., 2015; Grassani et al., 2016). As a result, the spectral purity of MRR-based sources is generally limited to 93%, requiring further engineering to modify the coupling conditions between the waveguide and the resonator for both the pump and biphoton fields (Vernon et al., 2017).

The use of pulsed excitation in photonic sources plays a central role for quantum communication and information processing applications, as this technique restricts the generation probability of quantum photonic states to discrete time windows (Brendel et al., 1999). This approach, known as time-bin encoding, provides several notable advantages. It is inherently robust to polarization fluctuations, a common issue in optical fibers, especially over long distances. Additionally, chromatic dispersion, which causes temporal spreading of photon wave packets due to wavelength-dependent velocities, can be passively compensated using linear optical elements (Zbinden et al., 2001). Time-bin encoding also enhances noise mitigation through temporal gating (Ribordy et al., 1998), enabling systems to effectively distinguish desired signals from noise and improve signal-to-noise ratios. Its compatibility with existing optical fiber infrastructures makes it ideal for long-distance quantum communication, including quantum key distribution (QKD) (Fitzke et al., 2022; Islam et al., 2017) and teleportation (Sun et al., 2016; Valivarthi et al., 2016; Shen et al., 2023). Pulsed excitation is a fundamental requirement for entanglement preparation in discrete temporal domains–time-bin entanglement (Brendel et al., 1999; Marcikic et al., 2002) – where the generated photonic state exists in a superposition of two or more time modes. This technique has also been employed for generating discrete frequency-entangled states in the telecom domain, allowing for their easy characterization through frequency mixing operations using electro-optic modulation (Kues et al., 2017).

Time-bin encoding, while highly robust against decoherence in optical fibers, faces several challenges. Measurements in the temporal domain rely on interferometric setups that demand ultrahigh phase stability (Cho and Noh, 2009; Pulford et al., 2005; Toliver et al., 2015; Martin and Jiang, 2010), as even minor environmental fluctuations can disrupt coherence and reduce quantum state fidelity. Although integration with on-chip platforms offers a promising solution, achieving precise time delays and phase control within compact designs remains a significant challenge (Xiong et al., 2015; Zhang et al., 2018; Thiel et al., 2024). Scaling to multi-photon or higher-dimensional systems introduces further challenges (Yu et al., 2024; Yu et al., 2025), such as maintaining coherence across multiple time bins, managing crosstalk between adjacent bins, and the need for large and complex circuit architectures. Additionally, time-bin encoding in quantum repeater architectures is sensitive to losses during photon transmission or storage, necessitating highly efficient collection mechanisms (Appel et al., 2022). Reliable performance also depends on high-resolution single-photon detectors with minimal timing jitter, as detection inefficiencies can degrade measurement accuracy (Bouchard et al., 2023). Lastly, validating complex time-bin encoded states, especially in higher-dimensional systems, often demands resource-intensive methods such as quantum state tomography or witness operators, adding experimental complexity (Sciara et al., 2019). Nonetheless, advancements in stabilization techniques, detector technologies, and integrated photonics are driving progress toward overcoming these limitations.

This paper reviews the use of two parametric photon sources for time-bin encoding, high index doped silica glass MRRs for photon pair generation via SFWM and periodically poled lithium niobate (PPLN) waveguides for SPDC. These complementary platforms have enabled diverse quantum state generation methods for time-bin encoding. The MRR platform supported pulsed quantum frequency combs for the generation of co- and cross-polarized correlated states, as well as multi-photon time-bin entangled and cluster states with higher-dimensional time-frequency entanglement. To characterize these states accurately, ultrastable fiber-based time-bin analyzers, supported by a bi-chromatic reference signal, were utilized to maintain stability and resolve phase ambiguities inherent in interferometric schemes. The PPLN platform, on the other hand, was used alongside a fiber-based coupled-loop architecture to create a

10.3389/aot.2025.1560084

synthetic photonic lattice in the temporal domain, i.e., a temporal photonic lattice. This configuration allowed for the resource-efficient generation of two- and four-dimensional time-bin entangled states, with dynamic control over photon propagation through an optical coupler, establishing a quantum walk architecture. Additionally, the use of on-chip higher-dimensional time-bin analyzers for the generation, processing, and application of time-bin entanglement is discussed, with a particular focus on quantum key distribution. Finally, we review a detection scheme that improved the resolution of time-correlated single-photon counting systems by employing a time-stretch sampling technique via electro-optic modulation, enabling precise temporal measurements. Together, these setups, built with readily available fiber-optic components and commercial photonic sources, represent significant advancements toward practical, scalable and cost-effective quantum photonic technologies for a wide range of applications in the temporal domain.

2 Parametric photon sources

Engineered photonic sources are essential for generating quantum-correlated and entangled states through parametric processes. The resulting photon pairs obey two fundamental laws: energy and momentum conservation. For SPDC (SFWM), these laws are represented as $\omega_p = \omega_s + \omega_i$ ($2\omega_p = \omega_s + \omega_i$) and $\overrightarrow{k_p} = \overrightarrow{k_s} + \overrightarrow{k_i}$ ($2\overrightarrow{k_p} = \overrightarrow{k_s} + \overrightarrow{k_i}$), respectively, where ω denotes the angular frequency, $\vec{k}$ is the wave vector, and the subscripts p, s, and i correspond to the pump, signal, and idler fields. Momentum conservation, achieved through phase matching, is crucial as it ensures efficient nonlinear frequency conversion between the interacting fields and determines the properties of the photon pairs, including emission angles, polarization, and wavelength. SPDC occurs in non-centrosymmetric materials exhibiting second-order nonlinearity ($\chi^{(2)}$), while SFWM occurs in centrosymmetric materials governed by third-order nonlinearity ($\chi^{(3)}$). Various parametric sources have been realized in dielectrics (Kwiat et al., 1999; Kultavewuti et al., 2017; Shukla and Ghosh, 2020; Sansoni et al., 2017; Montaut et al., 2017; Vallés et al., 2013; Finco et al., 2024), semiconductors (Appas et al., 2021; Sultanov et al., 2022; Zeng et al., 2024), as well as CMOS integrated (Takesue et al., 2008; Takesue et al., 2007; Lv et al., 2013; Zhang et al., 2024) and fiber (Goldschmidt et al., 2008; Smith et al., 2009; Chen C. et al., 2021) based platforms.

In parametric processes, biphotons are emitted coherently at distinct times within the pump coherence period, creating ambiguity in the exact emission time of each pair. This temporal uncertainty, coupled with strict energy constraints that maintain strong spectral correlations, naturally produces energy-time entangled photon pairs (Franson, 1989). The biphoton emission from parametric processes can be described as a superposition of photon number states, where there is a certain probability of generating one or more photon pairs. This means that while single photon-pair generation is most common, there is always a chance of producing multiple photon pairs during each pump excitation. These multi-photon events can introduce noise and degrade the quality of entanglement (Marcikic et al., 2002). To minimize this issue, the probability of generating photon pairs is kept low, with an average of no more than 0.1 signal/idler pairs per pump pulse (or per temporal window over which photons are detected).

Parametric processes are commonly classified into three types: type-0 and type-I, where the signal and idler photons share the same polarization, and type-II, where the photons have orthogonal polarizations. Type-II schemes offer significant advantages for collecting photon pairs in degenerate (where the signal and idler photons have the same energy) configurations, as the photons can be separated by polarization, unlike type-0/I schemes, which rely on 3-dB couplers to split degenerate photons (Tanzilli et al., 2002). Hence, type-0/I schemes are often preferred for generating non-degenerate (where the signal and idler photons have different energies) photon pairs (Friberg et al., 1985). In terms of efficiency, type-0/I processes in established materials like lithium niobate and potassium titanyl phosphate are more effective than type-II processes due to their high nonlinear coefficients. However, recent advances in platforms like aluminum gallium arsenide have demonstrated strong type-II nonlinearities (Appas et al., 2021), making them promising candidates for CMOS-compatible integrated photonic circuits that can inherently generate polarization entanglement. The variety of phase matching options available with parametric photonic sources provides flexibility in designing photon pair sources, allowing optimization based on the specific requirements of quantum experiments or applications.

2.1 Pulsed operation of parametric sources

Pulsed excitation is essential for encoding quantum states and preparing entanglement within discrete temporal domains, time-bin entanglement (Brendel et al., 1999; Marcikic et al., 2002). There are three main methods to develop pulsed excitation schemes. The first method relies on using an unbalanced interferometer to split an incoming laser pulse into multiple pulses with a well-defined time delay. Here, the coherence length of the incoming laser pulse is much greater than the delay between the two pulses, ensuring phase stability. The amplitudes in this case need to be balanced out, which is why active tuning of the splitting components in the interferometer is a crucial requirement. When realized in fiber-optic and free-space platforms, this pumping scheme is typically used to generate lower-dimensional time-bin entanglement, i.e., 2, 3, or 4-dimensions. However, with mature chip-based technologies, the dimensionality of such a pumping scheme have been greatly enhanced, now providing 8-dimensional time-bin entanglement using a cascade of three unbalanced Mach-Zehnder interferometers (Yu et al., 2025). The second excitation scheme utilizes a carved continuous-wave (CW) laser output, achieved through electro-optic modulation, to produce coherent pulses (Islam et al., 2017). This approach simplifies the overall setup by eliminating the need for interferometers in pump preparation, while also enabling efficient integration of pump sources into a compact and integrated design (Shams-Ansari et al., 2022). The third excitation method exploits a sequential pumping scheme (Stucki et al., 2005; De Riedmatten et al., 2004; Zhang et al., 2008), where a train of evenly spaced pulses emitted from a mode-locked laser is used, thus maintaining phase coherence between the pulses (see Figure 1a). This setup generates a more complex quantum state across multiple time bins, extending the concept of time-bin entanglement to higher dimensionalities. It allows for the generation of sequentially entangled photon pairs at much higher clock rates, in the GHz regimes (Zhang et al., 2008). Unlike the other schemes, photon correlations are observed in all time bins, except the first and last bins. An

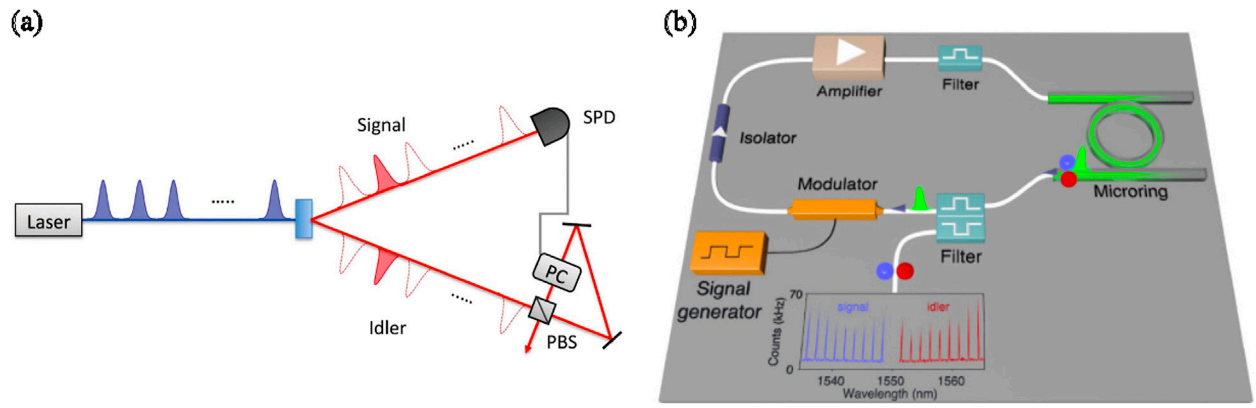

FIGURE 1
Experimental schemes for pulsed excitation of parametric optical sources. **(a)** Setup includes a bulky mode-locked laser for sequentially pumping a nonlinear optical source to produce photon pair states. PBC, polarizing beam-splitter; PC, Pockels cell; SPD, single-photon detector. Reprinted with permission from Ref (Kaneda et al., 2015). © Optical Society of America. **(b)** Setup used for the generation of quantum frequency combs using an intra-cavity mode-locked scheme, realized without the use of an external laser. Reprinted with permission from Ref. (Roztocki et al., 2017).

alternative and less commonly used pumping scheme for generating time-bin entanglement utilizes the coherence revival property of multimode continuous-wave laser sources (Kwon et al., 2009). This property allows multimode lasers to exhibit coherent behavior at specific intervals when the longitudinal modes periodically align, determined by the length of the laser cavity. In this scheme, time-bin entangled states are produced with a temporal separation that corresponds to an integer multiple of the coherence revival time of the laser.

In the case of MRRs, pulsed excitation can lead to the emission of high-quality, spectrally pure, pulsed QFCs, which contribute as valuable resources for multi-photon interference experiments (Silverstone et al., 2015; Faruque et al., 2018; Zhu et al., 2020; Heuck et al., 2019) as well as for implementations of quantum computation, teleportation, and secure communication protocols (Llewellyn et al., 2020; Scott et al., 2019; Bawankar and Singh, 2021; Yao et al., 2018). However, when considering practical and scalable systems, pulsed excitation schemes are often unsuitable due to their reliance on bulky, expensive, and complex external laser sources. To enable the transition of integrated photonic sources like MRRs from laboratory-based environments to real-world scenarios, it is crucial to realize versatile, stable, and low-power approaches for pulsed pumping operations. Addressing this challenge, this review presents a pulsed excitation technique known as the intra-cavity mode-locked scheme, for generating correlated photon pairs using MRRs, eliminating the need for an external laser. The developed scheme offers a scalable means to improve photon generation rates without compromising the device signal-to-noise ratio by leveraging standard components only from the telecommunications and integrated photonics domains.

2.2 Generation of pulsed quantum frequency combs

The experimental setup for the intra-cavity mode-locked architecture is depicted in Figure 1b. The excitation of a MRR to generate pulsed QFCs was accomplished using a nested fiber-loop configuration. The external fiber cavity consisted of an optical gain component, an erbium-doped fiber amplifier, and an active amplitude modulation element to enable pulsed pumping. This approach, known as the intra-cavity mode-locked scheme, allowed for the oscillation of multiple external fiber cavity modes within the resonance bandwidth of the MRR, depending on the fiber-loop length (Roztocki et al., 2017). By applying a modulation signal matching the frequency of the external mode spacing, a phase-locked configuration with a repetition rate corresponding to the modulation frequency was achieved. Notably, this implementation represents the first instance of generating pulsed QFCs without relying on an external laser-based pump source, offering an affordable and practical framework for developing fiber-integrated chip-based quantum photonic resources.

The performance of the mode-locked scheme as a reliable platform for quantum state preparation was evaluated through non-classical measurements performed on the generated photon pairs. Of interest is the operational metric coincidences-to-accidentals ratio (CAR), which quantifies the signal-to-noise ratio in quantum sources. In pulsed schemes, the CAR is determined by taking into account the number of signal/idler coincidence events recorded for the same pump excitation pulse (CC) and the events from different excitation pulses (AC). The coincidences-to-accidentals ratio is given by $CAR = \frac{CC-AC}{AC}$, and is highly influenced by the excitation conditions, such as pump power, and the level of noise in the system. A high CAR value of 110 was achieved, highlighting the potential of the mode-locked scheme to reliably generate quantum photonic states while maintaining a simple and energy-efficient implementation. A notable feature of the presented scheme is its flexibility in QFC generation rates obtained by tailoring the modulation frequency, and consequently, the repetition rate of the scheme. This was achieved by simply driving the active amplitude modulation element with harmonic frequencies of the external cavity mode spacing, requiring no modifications to the setup layout. As an additional advantage, the harmonic pulsing of the scheme retained the CAR values (as the energy per pulse remained constant), while enhancing the photon pair generation rates. These results clearly demonstrated the scalability and versatility of the intra-cavity mode-locked scheme, making it suitable for practical architectures and facilitating the commercialization of quantum light sources.

The intra-cavity mode-locked scheme, in conjunction with an external CW laser, was also utilized to generate cross-polarized states (through a type-II SFWM process) (Reimer et al., 2015), where the individual signal/idler modes could be separated via a polarization optical beam splitter. The hybrid bi-chromatic pumping architecture was tailored to independently excite each of the two polarization modes (transverse electric, TE, and transverse magnetic, TM) of the MRR, where cross-polarized photon pairs were generated only when both orthogonally-polarized pump fields triggered SFWM processes. This method ensured that stimulated emissions were suppressed as the resultant frequency bands (which need to be symmetric with respect to the two pump frequencies) did not overlap with the transmission bands of the MRR resonances. Here, a quadratic scaling in the coincidence events (characteristic of SFWM processes) was observed only when the powers of both pump fields were simultaneously increased. The spectral purity and single-photon operation of the platform was evaluated through unconditioned and conditioned second-order autocorrelation function ($g^{(2)}$) measurements with a Hanbury Brown and Twiss setup (Brown and Twiss, 1956). A high spectral purity value, close to the ideal value of 1, was recorded, indicating the quality of the photonic scheme to generate single-mode quantum states in the frequency domain, a crucial resource for quantum interference experiments (Silverstone et al., 2015; Faruque et al., 2018; Zhu et al., 2020; Heuck et al., 2019). A conditioned $g^{(2)}(0)$ value of 0.26 was also measured, well below the threshold value of 0.5 (Leifgen et al., 2014), signifying non-classical operation of the source. These measured performance metrics underscore the feasibility and practicality of generating cross-polarized photon states using standard telecom-based fiber-optic components and a silicon-based MRR source. Further enhancements to the platform design can be envisioned by incorporating chip-integrated optical elements for spectral filtering and polarization-dependent routing, such as dense wavelength-division multiplexers and polarization optical beam splitters, respectively, for efficient processing of the generated cross-polarized photon states.

3 Entanglement

Various quantum photonic applications have been prompted by entanglement, non-classical correlations in multi-partite quantum systems where the state or wavefunction of each particle cannot be described independently without considering the state of the others. Entanglement also serves as a potential resource for scalable and cost-effective quantum technologies (Arrazola et al., 2021; Chen and Segev, 2021), particularly when implemented using integrated architectures. Bell (i.e., maximally-entangled) states (Zhang et al., 2019; Kim et al., 2001) have been successfully prepared and processed using on-chip (Clementi et al., 2023; Bawankar and Singh, 2021; Yao et al., 2018) and fiber-based (Zhu et al., 2012; Chen et al., 2022) platforms. Bell states have also become indispensable for other quantum communication protocols, including quantum state teleportation (Yin et al., 2012; Kim et al., 2001; Pirandola et al., 2015; Luo et al., 2019; Wang and Yan, 2016) and super-dense coding (Barreiro et al., 2008). Unlike single-photon based approaches (Liao et al., 2017; Wang et al., 2013), platforms based on Bell states enable the realization of device-independent communication networks, eliminating the requirement for trusted quantum sources in QKD systems (Slater et al., 2014). Moreover, when combined with the advantages of qudit states, higher-dimensional entanglement-based quantum communication schemes exhibit greater noise resilience compared to standard qubit-based architectures with equivalent dimensionalities (Cozzolino et al., 2019; Ecker et al., 2019).

Entanglement also plays a crucial role in quantum computation tasks, particularly for the implementation of measurement-based (or one-way) quantum computers, which rely on the use of cluster states as a computational resource (Briegel and Raussendorf, 2001; Zhou et al., 2003; Walther et al., 2005a; Raussendorf and Briegel, 2001). Cluster states are a unique class of multi-partite entangled states that exhibit maximal connectedness, which implies that by performing projection measurements on any pair of the cluster state, the remaining qubits/qudits collapse into maximally entangled states pairwise. Furthermore, these states show high persistency of entanglement, meaning, a larger number of projection measurements is required to disentangle cluster states compared to other entangled states having the same number of parties. These properties are at the basis of the computational approach of so-called one-way quantum computers (Raussendorf and Briegel, 2001). Cluster states are used to encode information, which is subsequently read out through projection measurements on individual photon states composing the cluster after specific processing steps. This implies that, despite the complexity involved in generating high-fidelity cluster states, the computing operations (i.e., projections) are relatively easy to implement.

3.1 Pulsed energy-time entanglement—Time-bin entanglement

Time-bin entanglement is a discrete form of energy-time entanglement, where the involved states are defined by distinct, non-overlapping time intervals, allowing for precise control and robustness in applications including quantum key distribution (Chapman et al., 2022; Vagniluca et al., 2020), cryptography (Tittel et al., 2000), teleportation (Sun et al., 2016; Anderson et al., 2020), and computing (Humphreys et al., 2013). In qubit-based architectures, time-bin entanglement is produced by exciting a photon source with two consecutive laser pulses. To ensure a stable phase relationship between the pulses, the coherence length of the pump laser must be significantly longer than the time interval between them. Each laser pulse initiates a nonlinear optical process, SPDC or SFWM, with a certain probability of generating an entangled photon pair. When the system is driven with a very low excitation probability, on average, only one of the two pulses will generate a photon pair. This places the system in a superposition state, excited by either the early or the late pulse. Each photon pair can then be represented as time-bin qubits, where the early temporal mode is denoted by $|0\rangle$ and the late mode by $|1\rangle$. A time-bin entangled qubit is expressed as $|\psi\rangle = \frac{1}{\sqrt{2}} \left(|0,0\rangle_{s,i} + e^{i\phi_0} |1,1\rangle_{s,i} \right)$, where ϕ_0 represents the relative phase between the two temporal modes. The quality of the entanglement is typically verified through quantum interference and quantum state tomography measurements.

The first realization of time-bin entangled states was demonstrated in (Brendel et al., 1999), using a lithium niobate crystal, to overcome decoherence in polarization-encoded quantum communication over long-distance fibers. A key element for time-bin entanglement is a 1-bit delayed interferometer, often implemented through unbalanced Michelson and Mach-Zehnder interferometers, used as a Franson interferometer (Franson, 1989). The difference between Franson interference in CW laser-pumped energy-time entanglement and pulsed laser-pumped time-bin entanglement is that while the former only requires two-fold coincidence counts, the latter requires a synchronous signal for accurate coincidence measurements. In time-bin entanglement, if only two-fold coincidence counts are recorded, the result is a three-peak histogram, where the first and last time slots correspond to photon pairs traveling through different interferometric paths. The central peak in this histogram includes four types of events: (i) two photons generated in the early bin taking the short paths, (ii) two photons generated in the late bin taking the long paths, (iii) two photons generated in the early bin taking the long paths, and (iv) two photons generated in the late bin taking the short paths. Only the third and fourth events are indistinguishable and can interfere, which results in a maximum interference visibility of 50% for two-photon coincidence measurements. The solution is to introduce a synchronous signal which allows for the splitting of the central peak of the two-photon coincidence histogram into three distinct time slots. The side time slots correspond to the first and second events, while the middle slot corresponds to the indistinguishable third and fourth events, thus raising the theoretical visibility of Franson interference to 100% (Marcikic et al., 2002). The detection probability of the interfered state is described by, $P(\phi) \propto 1 + V\cos\phi$, where V represents the interference visibility and ϕ is the phase shift introduced by the interferometer, given by the sum of the signal and idler phases, $\phi = \phi_s + \phi_i$. By measuring the coincidence detection rate as a function of the phase shift ϕ, quantum interference can be observed. The interference visibility is directly related to the degree of entanglement between the photon pairs. High visibility indicates strong phase coherence and robust time-bin entanglement, while reduced visibility suggests the presence of decoherence or system noise, often caused by multi-photon emissions and parasitic processes in quantum systems.

Quantum state tomography (QST) for time-bin entangled qubits is performed using 1-bit delayed interferometers to carry out projection measurements, allowing the reconstruction of the full density matrix of entangled states (Takesue and Noguchi, 2009). To execute QST, various basis states need to be measured, including the time basis, which involves determining whether the photon is in the early or late temporal modes, and the energy basis, which involves measuring superposition states $|+\rangle = \frac{|0\rangle+|1\rangle}{\sqrt{2}}$ and $|L\rangle = \frac{|0\rangle+i|1\rangle}{\sqrt{2}}$. These basis measurements can be achieved through projection measurements by applying appropriate phase shifts between the interferometer arms. In total, a minimum of 16 projection measurements are required to reconstruct the complete 4×4 density matrix for a pair of time-bin entangled photons, where each photon is projected onto the states $|0\rangle$, $|1\rangle$, $|+\rangle$, and $|L\rangle$. Notably, all the necessary projections can be realized using just four combinations of the energy basis for the photon pairs: $|++\rangle$, $|+L\rangle$, $|L+\rangle$, and $|LL\rangle$. Once all the projection measurements are performed, the results are used to reconstruct the density matrix, typically through a maximum likelihood estimation method. This method is used so that the reconstructed density matrix is physical, meaning it is Hermitian, positive semi-definite, and has a unit trace.

3.2 Qubit-based time-bin entanglement analyzers

Franson interferometers (Franson, 1989) for time-bin entanglement analysis have been developed in free-space (Thiel et al., 2024; Jin et al., 2019), fiber (Brendel et al., 1999; Hunault et al., 2010; Ono et al., 2024; Kim et al., 2024; Marcikic et al., 2004; Tittel et al., 1998), and chip-based (Reimer et al., 2016; Ikuta and Takesue, 2018; Finco et al., 2024) architectures. Recently, a fully integrated photonic chip on a lithium niobate-on-insulator (LNOI) platform was demonstrated (Finco et al., 2024), combining entanglement generation and processing on a single chip (see Figure 2a). This device incorporated all essential optical elements, from the photon source to the time-bin analyzers, requiring only an external pump laser and single-photon detectors. In this setup, pulsed laser light was coupled into the chip via focused grating couplers to pump a periodically poled lithium niobate waveguide, which generated photon pairs through SPDC. The photons were separated and processed through separate on-chip Franson interferometers. In each interferometer, the short arm included a variable optical attenuator to balance propagation losses and enhance quantum interference visibility. These attenuators were implemented as Mach-Zehnder interferometers with thermo-optic phase shifters, while additional phase shifters in the delay line adjusted the signal and idler photon phases to enable accurate projection measurements. This design achieved a visibility of 78.1%, limited mainly by chromatic dispersion, with QST measurements showing a fidelity of 91.9%. This integration of time-bin entangled qubit generation and analysis on an LNOI chip is a first, taking advantage of LNOI's low propagation loss, wide transparency range, and extensive electro-optic bandwidth, making it a promising platform for scalable quantum technologies.

Commercially available interferometers have been effectively used to generate and characterize time-bin entanglement without active temperature control or feedback (Mueller et al., 2024). Their compact size (providing picosecond temporal separations) and temperature stability allow minimal phase drift, supporting reliable, high-visibility quantum interference in time-bin entanglement analysis. Using a frequency-multiplexed setup with eight time-bin entangled photon pairs, such configurations have achieved entanglement rates in the MHz regime with interference visibilities over 99%, marking a significant step toward practical, high-performance time-bin entanglement applications in quantum photonics.

3.2.1 Ultrastable fiber-based unbalanced Mach-Zehnder interferometer

Accurate measurements of quantum states rely on precise interferometric techniques, necessitating full control and stable

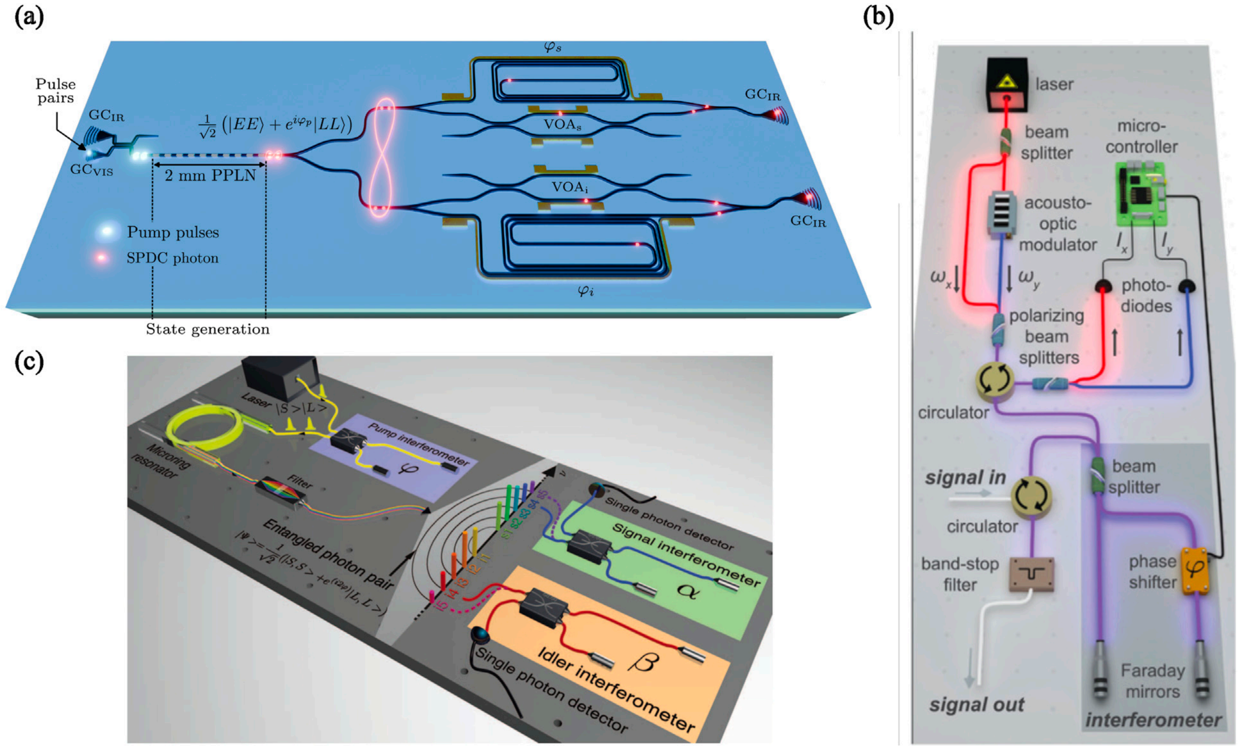

FIGURE 2
Qubit-based time-bin analyzers. **(a)** The time-bin analyzer is realized on an on-chip lithium niobate on insulator platform. Reprinted with permission from Ref. (Finco et al., 2024). GC, grating coupler; PPLN, periodically-poled lithium niobate; VOA, variable optical attenuator; φ, projection phase; s, signal; i, idler; p, pump; IR, infrared; vis, visible; E, early time mode; L, late time mode. **(b)** Fiber-based interferometer featuring a bi-chromatic pumping scheme for active stabilization. The frequencies ω_x and ω_y correspond to the two reference signals introduced into the interferometer, producing outputs I_x and I_y, respectively, which depend on the applied phase φ. Reprinted with permission from Ref. (Roztocki et al., 2021). **(c)** Time-bin entanglement scheme using the fiber-based interferometer shown in **(b)**. φ, α, and β are the phases applied to the pump, signal, and idler interferometers, respectively. $|S\rangle$ and $|L\rangle$ represents the time bins generated from the short and long arms of the interferometer, respectively. Reprinted with permission from Ref. (Reimer et al., 2016).

operation of unbalanced Mach-Zehnder interferometers (UMZIs). Several approaches have been employed to improve the stability of interferometers (Cho and Noh, 2009; Pulford et al., 2005; Toliver et al., 2015; Martin and Jiang, 2010), with one common technique involving the use of a CW reference laser to extract the interferometric phase (Cho and Noh, 2009; Pulford et al., 2005). However, this approach introduced ambiguities during phase retrieval as the monitored intensity, used to verify the interferometric stability, did not possess a one-to-one mapping with the phase. This means, when the interferometric phase was scanned from 0 to 2π, the recorded intensities showed similar values for various phase settings, e.g., for $\pi/2$ and $3\pi/2$. To address this ambiguity, active tuning of the interferometric delay or the wavelength of the reference laser has been proposed (Roztocki et al., 2021). However, implementing such procedures introduces additional experimental challenges, particularly in cases where synchronization of multiple UMZIs is required for time-bin entanglement characterization. The development of stable and unambiguous phase retrieval techniques remains an ongoing research area, aiming to improve the accuracy and reliability of quantum state measurements in UMZIs.

In (Roztocki et al., 2021), an ultra-stable UMZI scheme was developed, where the ambiguity in phase retrieval was eliminated by using a novel UMZI stabilization approach featuring a bi-chromatic reference signal (see Figure 2b). A single CW laser signal was divided into two fields: one field was left unaltered (in-phase signal), while the other field underwent acousto-optical modulation, inducing an optical frequency shift (quadrature signal). The frequency shift was carefully chosen to introduce a π/2 phase component to the quadrature signal relative to the in-phase signal. By simultaneously monitoring the phase-dependent in-phase and quadrature signals after passing through the UMZI, the bi-chromatic reference signal enabled the accurate determination of interferometric phase values. In the experimental setup, a UMZI with a 4 ns-delay was utilized, resulting in a frequency shift of 188 MHz for the quadrature signal with respect to the in-phase signal. Since the simultaneous measurement of both signals was necessary and commercial spectral filters were unable to separate such closely-spaced frequencies, the quadrature signal was prepared in the orthogonal polarization mode. This allowed for the simultaneous monitoring of both reference signals using a polarization optical beam splitter and two photodiodes. The proposed scheme demonstrated long-term stability, with an Allan deviation of $<1.3 \times 10^{-3}\pi$ rad over a measurement time ranging from 1 ms to 1.2 h. This signified the reliable and ultra-stable operation of the UMZI. Moreover, this approach can be realized with low-intensity light as well as pulsed reference signals (Roztocki et al., 2021), making it a versatile tool for quantum signal processing applications.

3.2.1.1 Generation and processing of multi-photon time-bin entangled qubits

Using the demonstrated ultra-stable UMZIs (Roztocki et al., 2021), time-bin entangled photon states generated from a MRR was prepared and processed (see Figure 2c). The quality of entanglement was verified by quantum interference and QST measurements, enabled via the processing of the signal/idler photon pairs using separate UMZIs with temporal imbalances identical to that of the pump. Two-level quantum interference measurements were performed on five resonance pairs, resulting in raw visibilities exceeding 82%, which on background subtraction revealed values surpassing 93%. These measured interference visibilities exceeded the threshold value of 71% defined by the two-level Bell inequality, confirming the presence of time-bin entanglement for all five signal-idler pairs. QST measurements yielded a fidelity of 96%, and after the entangled state was propagated through a 40-km fiber link, a high fidelity of 87% was measured, indicating that entanglement was preserved even after long distance transmission. This result demonstrated the robustness of the entangled state and its ability to withstand the challenges posed by fiber link transmission.

MRR architectures support operation over multiple modes, enabling the creation of multi-photon entangled states. By selecting two distinct signal-idler photon pairs ($(s1, i1)$ and $(s2, i2)$), two-photon qubit states were generated as $|\psi_1\rangle = \frac{1}{\sqrt{2}}\left(|0,0\rangle_{s1,i1} + e^{i\phi}|1,1\rangle_{s1,i1}\right)$ and $|\psi_2\rangle = \frac{1}{\sqrt{2}}\left(|0,0\rangle_{s2,i2} + e^{i\phi}|1,1\rangle_{s2,i2}\right)$. Post-selecting four-photon events, with one photon in each frequency channel, produced a four-photon time-bin entangled state,

$$\left|\psi_{4-\mathrm{phot}}\right\rangle = \frac{1}{2}\left(|0,0,0,0\rangle + e^{i\phi}|0,0,1,1\rangle + e^{i\phi}|1,1,0,0\rangle + e^{2i\phi}|1,1,1,1\rangle\right),$$

where each term in the ket notation specifies the temporal modes occupied by the photons in the sequence $s1$, $i1$, $s2$, and $i2$. Generation of this four-photon state required matching the coherence length of both photon pairs to the excitation field's coherence time, which was inherently satisfied by the MRR's uniform resonance bandwidths. Four-photon quantum interference measurements yielded a high raw visibility of 89% without compensating for background noise or losses, where high visibilities were achieved across various signal-idler frequencies. A fidelity of 64% was achieved through QST measurements, lowered by noise and measurement imperfections, still consistent with practical non-integrated sources.

3.2.2 Post-selection-free time-bin entanglement analyzers

As previously mentioned, when entangled states pass through 1-bit interferometers, photons are distributed across three time slots, but only the interfered time slot is utilized for entanglement analysis. This is because passive 3-dB beam splitters in unbalanced Mach-Zehnder interferometers separate half of the incoming photons into distinguishable time slots, limiting the quantum interference visibility to 50% and requiring temporal post-selection for optimal visibility. To address this, (Brendel et al., 1999) proposed the use of an active optical switch synchronized to guide the early photon along the long path and the late photon through the short path. The paths were then deterministically recombined with a passive beam splitter, fully utilizing photon detection statistics for interference measurements. Reference (Vedovato et al., 2018) demonstrated this approach by replacing the optical switch with a balanced beam splitter and a fast phase shifter synchronized with the pump, selectively routing photons along specific paths through specific phase settings and improving entanglement measurement efficiency (see Figure 3a).

An integrated photonics chip was developed to certify time-bin entanglement using a Hug interferometer (Santagiustina et al., 2024), traditionally employed for energy-time entanglement verification (Rossi et al., 2008; Cabello et al., 2009; Lima et al., 2010; Cuevas et al., 2013; Carvacho et al., 2015). This setup represented a novel application of the Hug interferometer, which, in contrast to the traditional Franson interferometer, only required local post-selection on single-photon temporal distributions rather than on the joint temporal distribution of the entangled state. In the Hug scheme, a time-bin entangled photon pair is split and directed into the two inputs of the interferometer, yielding three distinct measurement outcomes. First, when the early photon's short path aligns with the late photon's long path, detections occur at the same observer, i.e., a single beam splitter output. These detections, appearing in separate time bins, showed no interference since they result from independent processes. Second, when the early and late photons travel along the short and long paths, respectively, no interference is detected. These detections occur at different observers, corresponding to events from different beam splitter outputs. Only the third outcome reveals two-photon interference, occurring when the early photon takes the long path and the late photon takes the short path, producing detections at both observers. To accurately certify entanglement, post-selection on each observer's single-photon detection events was implemented to filter out non-interfering coincidences.

3.2.2.1 Temporal photonic lattice based post-selection-free time-bin analyzer

An alternative approach for post-selection-free measurements used temporal photonic lattices (TPLs) (Regensburger et al., 2012) based on discrete-time quantum walks (DTQWs) (Lovett et al., 2010; Jayakody et al., 2023). Here, the time-bin entangled states were generated from a PPLN waveguide (Monika et al., 2024). The complete system employed a fully fiber-based coupled-loop architecture (Schreiber et al., 2010), which enabled the preparation, manipulation, and measurement of time-bin entangled qubits (see Figure 3b). By leveraging the dynamic control of the quantum walk, the setup achieved quantum interference measurements without requiring post-selection, significantly improving detection efficiency. In the TPL framework, the state of a quantum walker (photon) can be described as: $|\psi\rangle = \sum \alpha_k|k\rangle$, where α_k is the probability amplitude of finding the walker in the mode $|k\rangle = |n\rangle_p|\sigma\rangle_c$. Here, $|n\rangle_p$ corresponds to the synthetic position, defined by the time bin, and $|\sigma_c\rangle$ denotes the coin state, representing the photon's path through the short or long fiber loops. The evolution of the quantum walker was driven by a unitary operator that combines the action of a coin operator $\hat{C}$ (determining the photon's path) and a shift operator $\hat{\mathcal{S}}$ (updating the photon's position in the synthetic temporal lattice). This unitary operator is given by $\hat{U} = \hat{\mathcal{S}}\hat{C}$, where,

$$\hat{\mathcal{S}} = \sum_n |n+1\rangle_p\langle n|_p \otimes |L\rangle_c\langle L|_c + |n-1\rangle_p\langle n|_p \otimes |S\rangle_c\langle S|_c.$$

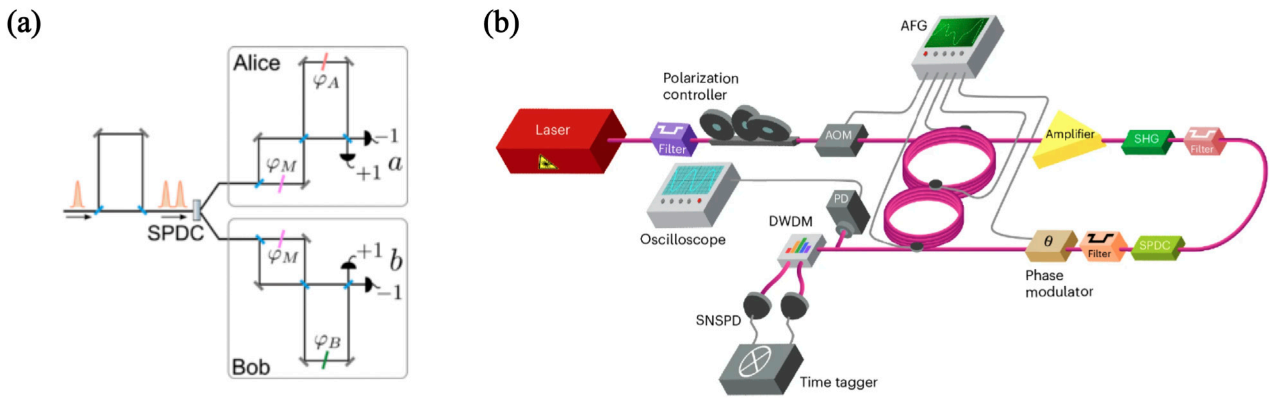

FIGURE 3
Post-selection-free time-bin entanglement analyzers. **(a)** Experimental scheme featuring a balanced Mach-Zehnder interferometer, instead of an optical switch, for selectively routing the time-bin states for optimized quantum interferometric processing using the phase modulator φ_M. The phase shifts φ_A and φ_B are applied to the local interferometers of Alice and Bob, with their interferometric outputs ($\pm$ 1) recorded by detectors labeled *a* and *b*, respectively. Reprinted with permission from Ref. (Vedovato et al., 2018). **(b)** Experimental scheme comprising a coupled-loop architecture for discrete-time quantum walk implementations, aimed at dynamically routing entangled photons. AOM, acousto-optic modulator; AFG, arbitrary function generator; SHG, second harmonic generation; SPDC, spontaneous parametric down-conversion; PD, photodiode; DWDM, dense wavelength division multiplexing; SNSPD, superconducting nanowire single-photon detector. Reprinted with permission from Ref. (Monika et al., 2024).

The shift operator dictates that the walker moves forward ($|n+1\rangle$) or backward ($|n-1\rangle$) in synthetic space (time bins) depending on the coin state (whether the photon takes the long $|L\rangle$ or short $|S\rangle$ loops). This modeled the time delays introduced by different loop lengths in the fiber setup. The coin operator, which controls the photon's path choice at each step (or round trips, m, in coupled-loop architectures) of the quantum walk, can be defined as

$$\hat{C}(n,m) = \begin{pmatrix} \cos\theta_{n,m} & j\sin\theta_{n,m} \\ j\sin\theta_{n,m} & \cos\theta_{n,m} \end{pmatrix},$$

where the angle $\theta_{n,m}$ controls the probability of the photon either being transmitted to the adjacent loop or being reflected back into the same loop. This operator determined the experimental transmission and reflection coefficients of the dynamic coupler in the fiber loops, allowing the creation of superpositions of paths for the quantum walker. The coupler supports three configurations: full reflection ($\hat{R}$; $\theta_{n,m}=0$), full transmission ($\hat{T}$; $\theta_{n,m}=\pi/2$), and 50:50 beam splitting (Fourier $\hat{F}$; $\theta_{n,m}=\pi/4$) operations. In the DTQW formalism, a time-bin entangled qubit state injected into the short loop can be represented as

$$|\psi\rangle = \frac{1}{\sqrt{2}}\left(|{-1}S\rangle_s|{-1}S\rangle_i + e^{i\phi}|1S\rangle_s|1S\rangle_i\right)$$

where the synthetic positions are $|n\rangle_p = \ldots, |-1\rangle, |0\rangle, |1\rangle, \ldots$

In a controlled DTQW scheme, post-selection-free quantum interference measurements were performed after two roundtrips of the photon pairs. During the first roundtrip, the coupler was set to transmit ($\hat{T}$) the early photon pair (at synthetic position $|-n\rangle$) into the long loop and reflect ($\hat{R}$) the late photon pair (at synthetic position $|n\rangle$) into the short loop. The corresponding unitary operator was,

$$\hat{U}_{TR} = \hat{S}_s.\left(\sum_n\left(|-n\rangle_p\langle -n|_p \otimes \hat{T}_s + |n\rangle_p\langle n|_p \otimes \hat{R}_s\right)\right) \otimes \hat{S}_i.\left(\sum_n\left(|-n\rangle_p\langle -n|_p \otimes \hat{T}_i + |n\rangle_p\langle n|_p \otimes \hat{R}_i\right)\right)$$

In the second round trip, the coupler was set to a 50:50 splitting ratio ($\hat{F}$), enabling quantum interference. The unitary operation for this step can be written as,

$$\hat{U}_F = \hat{S}_s.\left(\hat{\mathbb{I}}_p \otimes \hat{F}_s\right) \otimes \hat{S}_i.\left(\hat{\mathbb{I}}_p \otimes \hat{F}_i\right)$$

where $\hat{\mathbb{I}}_p$ is the identity over the position space. After two roundtrips, the evolved state was then given by $|\psi_2\rangle = \hat{U}_F\hat{U}_{TR}|\psi\rangle$. This dynamic tuning eliminated the need for post-selection, significantly reducing photon loss and resulting in more than a three-fold increase in the detected two-photon events compared to an uncontrolled/traditional approach. This scheme resulted in a high quantum interference visibility of 96.8%, exceeding the threshold of 71% for Bell inequality violation (Collins et al., 2002).

Figure 4 illustrates the improved two-photon detection efficiency achieved with post-selection-free time-bin analyzers, compared to the traditional Franson interferometer (Franson, 1989) and the Hug configuration (Santagiustina et al., 2024). Franson-based analyzers (Figure 4b) experience significant photon loss, necessitating extensive post-selection on both single-photon and two-photon detections, see Figure 4e. The Hug configuration, shown in Figure 4c, offers better efficiency, limiting post-selection to local single-photon detections but still incurs a 50% loss (see Figure 4f). In contrast, post-selection-free analyzers fully utilize all coincidence events without the need for post-selection, see Figures 4d, g, simplifying experimental procedures, reducing measurement time, and enhancing scalability for quantum information processing.

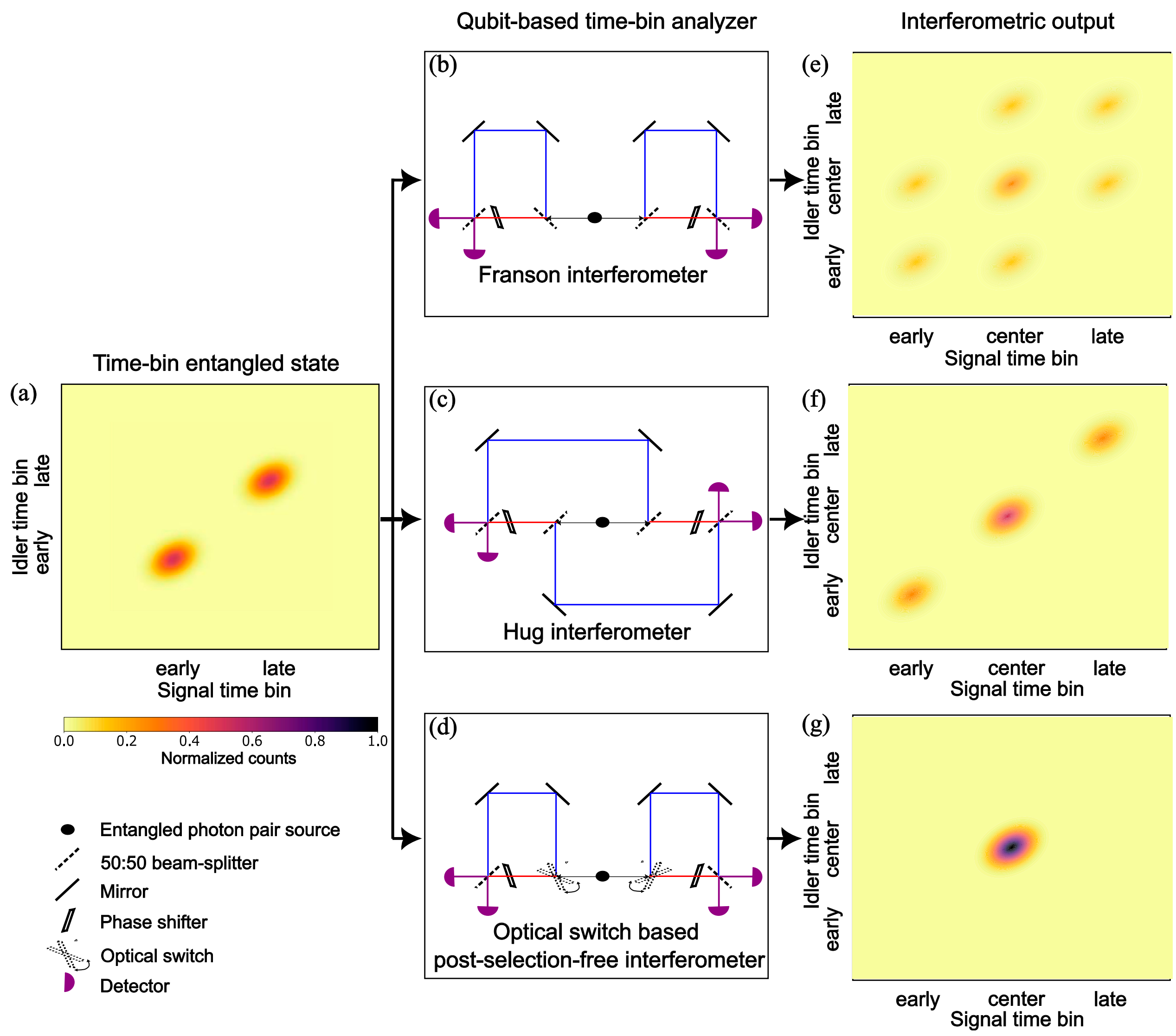

FIGURE 4
Comparison of qubit-based time-bin entanglement analyzers, illustrating the simulated two-photon coincidence distribution across time bins and the impact on entanglement characterization efficiency. **(a)** Time-bin entangled state generated from a photon pair source, which is then transmitted through an interferometer **(b-d)** for entanglement verification. The Franson-based analyzer **(b)** distributes two-photon detections across a central time bin (25% of coincidences) and six side bins (12.5% each), as shown in **(e)**. This results in a 75% coincidence loss and requires post-selection on the central time bin. The Hug configuration **(c)** improves efficiency by concentrating 50% of coincidences in the central bin and 25% in each of the two side bins as shown in **(f)**. Although post-selection remains necessary, it is limited to local single-photon detections. A conceptual post-selection-free analyzer is shown in **(d)**, which deterministically routes all photons into a single time bin, allowing complete utilization of coincidence events for entanglement characterization without post-selection (see **(g)**).

3.3 Higher-dimensional time-bin entanglement analyzers

Higher-dimensional time-bin entanglement analyzers are specialized devices designed to measure and process entangled states across multiple temporal modes, extending beyond the binary early-late time-bin encoding commonly used in quantum communication and quantum information protocols. These analyzers are typically implemented using cascaded unbalanced interferometers (Ikuta and Takesue, 2018; Yu et al., 2025), fiber-based interferometers (Thew et al., 2003; Fang et al., 2018) or coupled-loop architectures (Monika et al., 2024), with each stage introducing precise delays matched to specific time-bin separations (see Figures 5a–c). For example, a multi-arm interferometer, incorporating d optical delay lines and $d-1$ optical phase shifters, enables efficient discrimination of a d-level quantum state's temporal components, facilitating higher-dimensional Bell-type inequality measurements (Thew et al., 2003). Despite their potential, implementing higher-dimensional time-bin analyzers remains challenging, especially as dimensionality increases. Scalability requires precise control and stability, which become increasingly complex with added dimensions. Nevertheless, higher-dimensional time-bin analyzers offer substantial promise for advanced quantum applications, including higher-dimensional quantum key distribution, quantum error correction, and photonic quantum computing. These

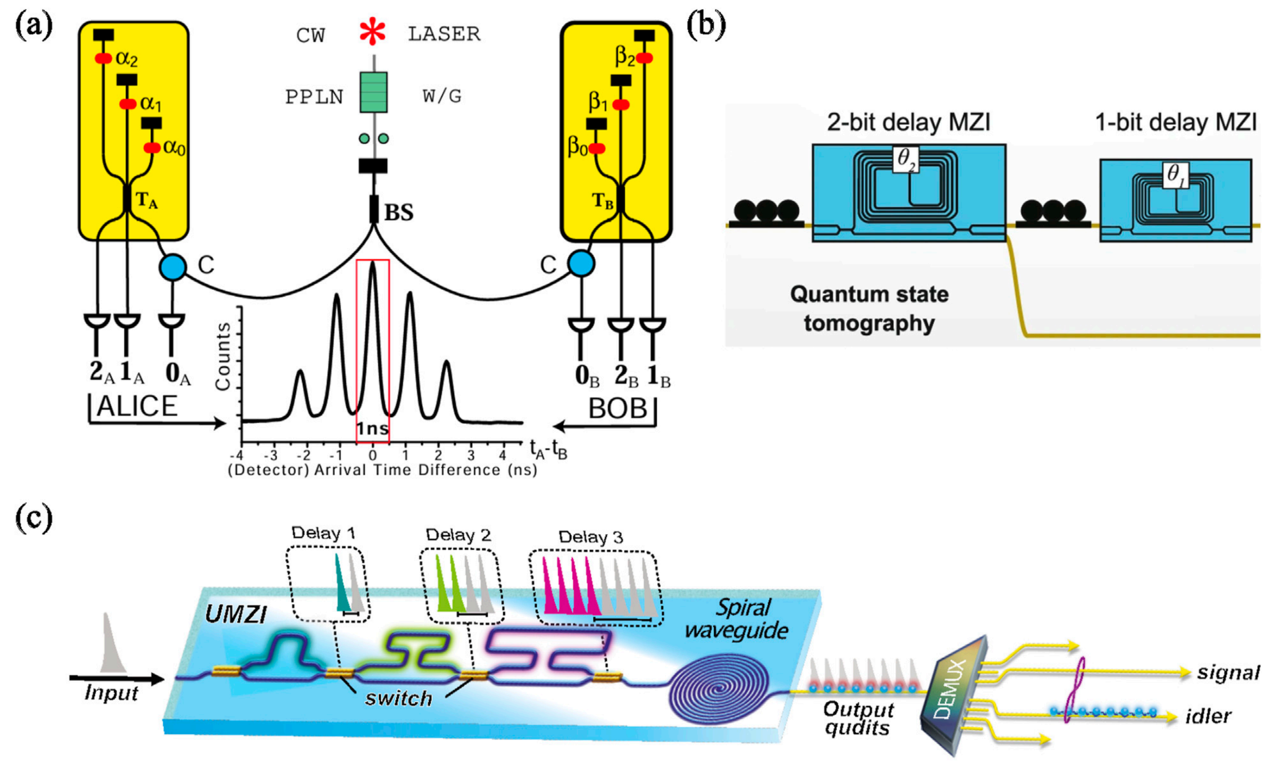

FIGURE 5
Higher-dimensional time-bin entanglement analyzers based on fiber-optics **(a)** and on-chip **(b, c)** platforms. CW laser, continuous-wave laser; PPLN w/g, periodically-poled lithium niobate waveguide; BS, beam-splitter; C, circulator; T_A and T_B, tritters (6-port symmetric couplers) with short (0), medium (1), and long (2) arms, incorporating phases α and β, used in the measurement stages of Alice and Bob, respectively; t_A and t_B, time-of-arrival measurements for Alice and Bob, respectively (U)MZI, (unbalanced) Mach Zehnder interferometer; DEMUX, demultiplexer. Reprinted with permission from Ref. (Ikuta and Takesue, 2018; Yu et al., 2025; Thew et al., 2003).

analyzers provide a versatile approach for processing quantum information with increased efficiency and security.

3.3.1 TPL-based higher-dimensional time-bin entanglement analyzer

The temporal photonic lattice (Monika et al., 2024) demonstrated in Section 3.2.2.1 showed scalability to higher-dimensional time-bin entanglement preparation and processing without relying on resource-intensive multiple-arm interferometers. In this work, four-dimensional time-bin entangled photon pairs were generated using a fiber-loop system, bypassing the need for complex setups. In the DTQW framework, the resultant entangled state can be represented as,

$$|\psi\rangle = \frac{1}{2}\left(|-3S\rangle_s|-3S\rangle_i + e^{i\phi}|-1S\rangle_s|-1S\rangle_i + e^{2i\phi}|1S\rangle_s|1S\rangle_i + e^{3i\phi}|3S\rangle_s|3S\rangle_i\right).$$

To implement quantum interference measurements for two-photon four-level states, two controlled DTQW strategies were used–the inter-roundtrip and intra-roundtrip schemes. The inter-roundtrip scheme involved fixing the coupler configuration within the same roundtrip and tuning it dynamically between roundtrips, while the intra-roundtrip dynamically tuned the coupler both within and between roundtrips. In the inter-roundtrip scheme, the coupler was set to a 50:50 split ($\hat{F}$) in the first two roundtrips, to full reflection ($\hat{R}$) in the third roundtrip, and back to 50:50 ($\hat{F}$) in the fourth roundtrip. After four roundtrips, the evolved state was then given by

$$|\psi_4^{inter}\rangle = \hat{U}_F\hat{U}_R\hat{U}_F\hat{U}_F|\psi\rangle,$$

where $\hat{U}_R = \hat{\mathcal{S}}_s.(\hat{\mathbb{I}}_p \otimes \hat{R}_s) \otimes \hat{\mathcal{S}}_i.(\hat{\mathbb{I}}_p \otimes \hat{R}_i)$. The photons were extracted from the short loop, and the central time bin was post-selected out of seven total bins (typically obtained from four-level entanglement). In the intra-coupler scheme, the central coupler was configured to transmit the first two time bins ($|-3\rangle$ and $|-1\rangle$) into the long loop and reflect the other two ($|1\rangle$ and $|3\rangle$) into the short loop. During the second roundtrip, the coupler reflected all four time bins within the loop they occupied in the previous step. In the last two roundtrips, the coupler was set to 50:50 to enable quantum interference. The evolved state can be then given by,

$$|\psi_4^{intra}\rangle = \hat{U}_F\hat{U}_F\hat{U}_R\hat{U}_{TR}|\psi\rangle.$$

The intra-coupler scheme reduced the number of time bin outputs to three (rather than seven), enhancing interference visibility by increasing the likelihood of overlap within the central time bin. Quantum interference measurements showed that this scheme enhanced coincidence counts by nearly two-fold compared to the inter-roundtrip scheme. Visibility values of 91.5% and 89.6% were obtained for the respective schemes, exceeding the threshold value of 81.7% for violating the Collins–Gisin–Linden–Massar–Popescu (CGLMP) inequality (Collins et al., 2002).

The proposed measurement strategy using TPLs can be theoretically extended to perform quantum interference and optimize detection efficiency for any number of levels (time bins). This approach offers the potential to inspire new designs for TPL systems capable of generating, processing, and detecting entangled modes with arbitrarily high dimensions, while maintaining maximum efficiency. This scalability opens opportunities for advanced quantum information processing and applications that require higher-dimensional entanglement.

3.3.2 Chip-based higher-dimensional time-bin entanglement analyzer

Yu et al. (2025) introduced a scalable integrated photonic platform for generating and processing four- and eight-level time-bin entangled photon pairs. The platform's core component was a cascade of programmable UMZIs integrated on a CMOS-compatible chip. These UMZIs provided precise control over input laser pulses, splitting them into coherent sequences to create time-bin entangled states via SFWM in a spiral waveguide (see Figure 5c). The system achieved time-bin spacings of 64 ps and 32 ps for four- and eight-level qudits, respectively, supporting processing rates on the order of 10s of GHz, consistent with modern optical communication systems. Notably, the platform maintained constant device loss irrespective of the quantum state dimensionality, an essential feature for scalable quantum systems. Although the UMZI cascade inherently supported scalability, maintaining phase coherence and minimizing losses at higher dimensions posed significant challenges. Despite these limitations, this work provided a robust and practical framework for higher-dimensional time-bin entanglement, offering a pathway toward high-rate quantum communications and highlighting its strong potential for integration into optical networks.

Despite the jitter time of single-photon detectors (~52 ps) being higher than the spacing between the time bins, it was still possible to resolve the entangled time bins through external temporal gating (Crockett et al., 2022) (see details on this methodology in Section 4). This technique enabled the post-selection of the time-bin modes through electronic gating, yet at the cost of introducing additional losses. The integrated platform, combined with external phase modulation and other fiber components (e.g., spectral filtering), enabled high quantum interference visibility, with measured visibilities of 90.1% and 91.2% for the four- and eight-level entangled states, respectively. These values exceeded the respective thresholds of 81.7% and 89.6% required to violate the CGLMP inequality, confirming the presence of higher-dimensional entanglement and the reliability of the platform.

The platform also demonstrated high quantum information density, a measure of encoding efficiency in the time-frequency space, given by $d^N/(\Delta t \times \Delta \nu)$, where d is the quantum state dimensionality, N is the photon number, Δt and $\Delta \nu$ are the time-bin and spectral bandwidths of the state. For the four- and eight-level biphoton states, the quantum information densities achieved were 0.156 and 0.625 per frequency channel with a bandwidth of 200 GHz, respectively, illustrating the platform's potential for high-data-rate quantum communications. To demonstrate a practical application, a BBM92-like QKD protocol was implemented using the generated four-level time-bin entangled states. The setup directed signal and idler photons to separate detection systems for Alice and Bob, enabling measurements in both the time basis (individual time bins) and the phase basis (superpositions of time bins). The system achieved quantum bit error rates of 10.97% and 13.05% for the time and phase bases, respectively, well below the threshold of 18.93% tolerated by four-level QKD protocols. Over 5 hours of operation, the platform produced an average secret key rate of 2.04 kbit/s, with potential for significant enhancement by mitigating losses from the external gating process required for picosecond temporal detection. To further validate the system's scalability and practicality, the BBM92 experiment was extended over a 60 km optical fiber link, achieving a raw visibility of 89.3% and a corresponding secret key rate of 37 bits/s. These results demonstrated the platform's capability for higher-dimensional entanglement generation and quantum key distribution, emphasizing its potential for high-rate quantum secure communication in metropolitan-scale optical networks.

3.4 Extension of time-bin entanglement to complex quantum systems

Cluster states, a class of complex highly-entangled multi-partite systems, serve as essential resources for various applications including one-way quantum computing (Briegel and Raussendorf, 2001; Raussendorf and Briegel, 2001), communication (Schlingemann and Werner, 2001; Cleve et al., 1999; Hillery et al., 1999), and error correction (Schlingemann and Werner, 2001). However, existing experimental methods for generating photonics-based cluster states face limitations in terms of multi-photon generation rates, predominantly due to the probabilistic nature of the parametric processes commonly used for entanglement preparation and of the fusion gate operations needed to produce the cluster states (Walther et al., 2005a; Walther et al., 2005b; Kiesel et al., 2005; Prevedel et al., 2007). A practical solution lies in leveraging hyper-entanglement (Kwiat, 1997), which enables the realization of cluster states using a reduced number of photons. Hyper-entangled states are multi-partite quantum systems that exhibit simultaneous entanglement in two or more independent DoFs (Chen et al., 2007; Vallone et al., 2008; Ciampini et al., 2016) that are experimentally separable, and, hence, measurements performed on one DoF do not impact the other. Furthermore, the use of hyper-entanglement for cluster state generation results in a significant reduction in the size and complexity of the photonic scheme (Reimer et al., 2019). This enhances photon detection rates, which scale with the number of photons p^N, where p represents the detection probability.

In (Reimer et al., 2019), four-partite three-level cluster states were generated by harnessing time-frequency hyper-entangled biphoton states. Time-bin entanglement was obtained by exciting a MRR with a sequence of three mode-locked pump pulses, while frequency-bin entanglement utilized three signal-idler resonances corresponding to the MRR's free spectral range. A necessary condition for achieving time-frequency hyper-entanglement is that the product of the temporal and spectral mode separations exceeds the Einstein-Podolsky-Rosen limit of one, ensuring robust quantum correlations (Franson, 1989). Satisfying this condition enabled the realization of four-partite three-level hyper-entangled states in the time and frequency domains. To transform this hyper-

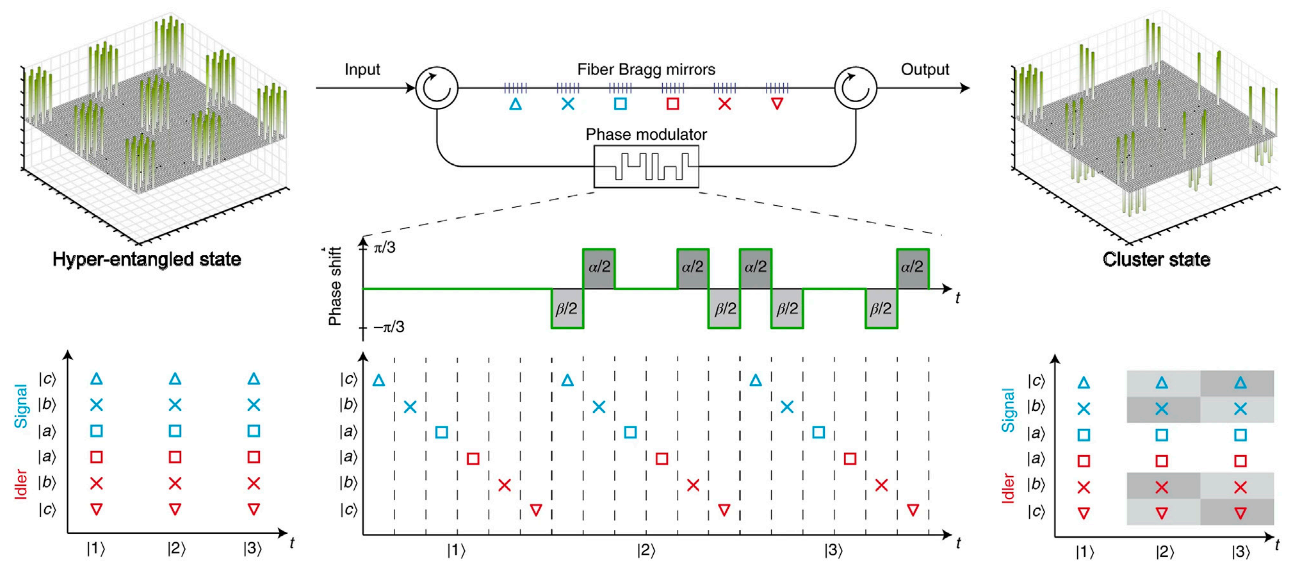

FIGURE 6
Controlled phase gate, comprising Fiber Bragg mirrors and an electro-optic modulator, utilized for transforming hyper-entangled states into four-partite three-dimensional cluster states. Adapted from Ref. (Reimer et al., 2019).

entangled state into a cluster state, specific phase factors were applied to certain frequency components using a custom-designed controlled-phase (C-phase) gate. This gate employed fiber-optic elements, including an array of six fiber Bragg gratings (FBGs) that matched the resonances of the signal-idler photons and an electro-optic phase modulator (see Figure 6). The spectral modes of the hyper-entangled state were reflected through the FBG array to perform frequency-to-time mapping. The phase modulator then introduced the desired phase factors to the frequency components, and the state was returned to the FBG array for the inverse mapping. This process successfully yielded the target cluster state, which was subsequently employed in a proof-of-principle demonstration of higher-dimensional one-way quantum operations. For further details on the generation and application of the cluster state, readers are directed to (Reimer et al., 2019).

To address the impracticality of QST for validating the genuine four-partite, three-level entanglement of the generated cluster state, a more efficient approach using witness operators was employed (Sciara et al., 2019). A witness operator, $\mathcal{W}$, is a Hermitian observable designed to estimate the degree of overlap between the measured and the ideal quantum state, as well as to determine the presence of entanglement. Importantly, the expectation value of $\mathcal{W}$ is non-negative for all separable states and becomes negative for specific entangled states, providing a clear criterion for entanglement verification (Tichy et al., 2011; Horodecki et al., 1996; Tóth and Gühne, 2005; Knips et al., 2016). In this study, universal witness operators were formulated, enabling entanglement characterization with a significantly reduced number of measurements compared to QST. A detailed theoretical approach for this method can be found in (Sciara et al., 2019). Using a set of specific projection measurements (for detailed information, see (Reimer et al., 2019)), the expectation value of $\mathcal{W}$ was determined with only 648 measurements, as opposed to the $d^{2N} = 6,561$ measurements required for full QST. The computed expectation value, $\langle \mathcal{W} \rangle = -0.28 \pm 0.04$, confirmed the presence of genuine four-partite three-level entanglement in the biphoton cluster state. This efficient validation method highlighted the practicality of using witness operators for complex high-dimensional quantum states.

4 Detection

Time-correlated single-photon counting (TCSPC) is crucial for accurately measuring time delays between single photons and a reference clock, enabling applications such as time-of-flight imaging (Barwicz et al., 2015; Torricelli et al., 2014; Gariepy et al., 2015; Shin et al., 2016; Rehain et al., 2020; Rapp et al., 2020), microscopy (Bruschini et al., 2019), fluorescence lifetime spectroscopy (Masters, 2014), and quantum information processing (Reimer et al., 2019; Lu et al., 2018; Zhang et al., 2015; Dixon et al., 2008; Lo et al., 2014; Valencia et al., 2002). In quantum processing, precise measurement of single-photon time differences relative to a reference determines how densely information can be encoded and retrieved over a quantum communication channel (Reimer et al., 2019; Lu et al., 2018; Zhang et al., 2015; Dixon et al., 2008; Lo et al., 2014). Additionally, the time delay distribution between joint detections of entangled photon pairs is critical for reconstructing the biphoton wavefunction (Valencia et al., 2002).

However, single-photon detectors often struggle with temporal resolution due to timing jitter. Recent advancements in superconducting nanowire single-photon detectors (SNSPDs) have achieved remarkably low jitter, down to 3 ps (Korzh et al., 2015), while commercial models typically reach 15 ps – 50 ps. However, SNSPDs require cryogenic cooling, making them impractical for many applications. On the other hand, single-photon avalanche diodes operate at room temperature and provides similar resolutions in the visible spectrum, but they perform less effectively in the near-infrared. To enhance resolution, nonlinear optical processes (Rehain et al., 2020; MacLean et al., 2018a; MacLean et al., 2018b; Allgaier et al., 2017; Kuzucu et al., 2008; Dayan et al., 2004; Lukens et al., 2014) have been exploited, achieving up to 1,000 times better resolution. However, this approach is complex and energy-intensive, making integration into compact systems challenging. Electro-optic methods (Mittal et al., 2017; Donohue et al., 2016; Harris, 2008; Belthangady et al., 2009; Lukens et al., 2015) offer modest enhancements, approximately 10 times, and are better suited for fiber and micro-optic applications, yet they remain limited in flexibility and application.

Bouchard et al. (2023) presented an experimental scheme for measuring ultrafast time-bin qudits, focusing on up to four dimensions, using compact and efficient techniques. Time-bin states were encoded in the picosecond timescale, with a bin separation of 2.6 ps, leveraging the small temporal spacing to enable compact UMZIs. The measurement system utilized birefringent crystals, α-barium borate (BBO), to introduce controlled group delays between orthogonal polarization states. This approach ensured intrinsic phase stability as all interferometric paths were maintained in a single spatial mode. The experimental setup employed two stages of nonlinear interaction for ultrafast polarization switching via cross-phase modulation induced by strong pump pulses. Specific time bins were selected and rotated in polarization, followed by recombination using BBO crystals. Temporal separation between bins was increased at each stage using polarization delays with path differences corresponding to nanosecond-scale shifts. This cascade of ultrafast interactions translated picosecond-separated time bins into nanosecond-scale intervals, compatible with standard single-photon detectors. This methodology effectively reduced the physical size of UMZIs to a few hundred micrometers, enhancing phase stability and compactness. The system achieved robust temporal separation of states while maintaining high fidelity in both computational and superposition bases measurements. The approach demonstrated a scalable framework for the precise manipulation and measurement of ultrafast time-bin qudits, paving the way for advancements in higher-dimensional temporal state manipulation.

4.1 Quantum optical sampling scope for ultrafast detection

Crockett et al. (2022) presented a technique aimed at improving the temporal resolution of single-photon detectors, making it applicable for TCSPC. The method utilized telecom-based electro-optic technology, specifically fiber-integrated intensity modulators and a commercial arbitrary waveform generator (AWG), to accurately resolve photon distributions with sharp temporal features, even when using detectors with lower temporal resolution. SNSPDs which showed a distorted instrument response function (IRF) extending over 1 ns were used, to resolve features as fast as 60 ps.

The concept is based on the electro-optic sampling time-stretch method used for ultrafast classical optical fields (Kanada and Franzen, 1986; Nikles et al., 1995), see Figure 7a, but adapted for single-photon waveforms. This method employed a periodic input signal with a temporal duration of T_0, which was divided into n intervals using an electro-optic gate with width T_0/n and period T_g (defined as $T_g = T_0 + T_0/n$). This created a stretched waveform, where a larger n resulted in greater stretching. The output signal duration, $T_s = nT_g$, corresponded to a stretch factor of $S = T_s/T_0$. This method improved the sampling resolution of slower detectors based on the degree of stretching. The achievable stretch factors were constrained by the gate width T_0/n, which was limited by the bandwidth of the AWG. Although this method significantly enhanced temporal resolution, it also increased acquisition times–a typical limitation of gating-based techniques. Nevertheless, an interleaved sampling approach (see Figure 7b) can mitigate the required integration time by sampling multiple segments of the temporal waveform within a single period T_0, improving efficiency for high time-bandwidth product (TBP) signals. The versatility of the technique was demonstrated by resolving various single-photon waveforms, including exponential decays and double-pulse signals that slow detectors could not directly detect. Using a stretch factor of $S = 97$, the system retrieved an exponential decay profile with high fidelity, achieving a Pearson correlation of 0.98, in contrast to 0.83 for the raw SNSPD response. Interleaved sampling was also utilized to recover a high-TBP data signal, demonstrating the method's capability to manage high-speed waveforms. For instance, a pseudo-random bit sequence signal at 10.8 Gb/s was successfully recovered with a stretch factor of $S = 73$, achieving a correlation coefficient of 0.93 compared to just 0.51 without sampling.

Additionally, the electro-optic gating method was applied to measure a biphoton waveform generated through SPDC, achieving a resolution 15 times better than the detection system's IRF. To obtain the desired biphoton temporal signal with features of approximately 100 ps, two frequency bins were filtered using a programmable Waveshaper and group velocity dispersion (GVD) was introduced through a single-mode fiber. This procedure mapped the spectral information to the time domain, producing a double-pulse biphoton waveform. The electro-optic gating system scanned the signal and idler waveforms simultaneously, with a stretch factor of $S = 49$ and a gate width of 98 ps, enabling the reconstruction of a 2D biphoton distribution that revealed the detailed double-pulse structure. Without the sampling technique, the 2D biphoton distribution, measured directly from the SNSPDs, showed no discernible features due to the broad IRF of the detectors. The technique also allowed for the observation of nonlocal dispersion cancellation (NDC) (Franson, 1992), a quantum phenomenon where applying opposite dispersion to the signal and idler photons cancels temporal broadening despite the photons being spatially separated. By applying different amounts of GVD to the biphotons, the NDC effect was demonstrated. The unsampled detection system could not resolve the dispersion-induced features, but the sampled waveforms revealed the expected biphoton distributions, with temporal resolutions of 98 ps.

Overall, the quantum optical sampling scope provided a simple and scalable solution to improve the resolution of single-photon detectors and enable the measurement of ultrafast quantum optical signals (refer to the experimental implementation in Section 3.3.2). By integrating off-the-shelf components and adapting classical optical techniques for quantum applications, the method enabled

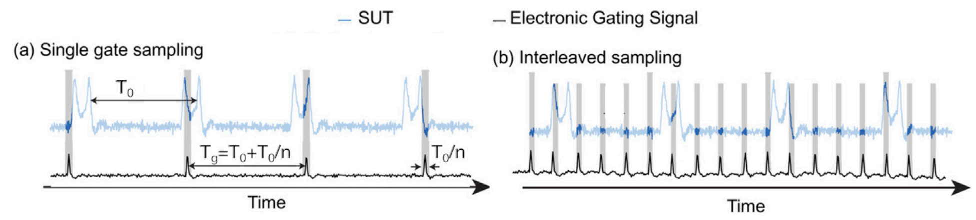

FIGURE 7
Time-stretch technique implemented by periodically sampling the signal under test (SUT): **(a)** basic concept, **(b)** interleaved approach. Adapted from Ref. (Crockett et al., 2022). The variables are defined in the main text of Section 4.

high-precision measurements. It offered practical advantages, as it could be integrated on-chip with modulation speeds greater than 100 GHz (Kharel et al., 2021; Benea-Chelmus et al., 2018; Burla et al., 2019), potentially achieving resolutions below 10 ps. These results showcased the ability of electro-optic sampling to resolve fine temporal details in biphoton waveforms, significantly improving resolution and allowing for the measurement of quantum phenomena like NDC that are otherwise unresolvable with conventional detection systems.

5 Discussion and conclusion

The adoption of integrated, CMOS-compatible quantum platforms for the generation of non-classical photonic states, combined with the use of commercially available fiber-optic components for their coherent processing, offers simple, low-footprint, and practical solutions to extend the application of quantum technologies on a global scale. In the field of quantum communication, polarization-encoded photon states (two-level schemes) have enabled practical demonstrations of space-to-ground quantum secure communication (Yin et al., 2017; Liao et al., 2017); however, only proof-of-concept quantum communication protocols have been implemented in the domains of time- and frequency-entanglement (two- and high-level schemes). The presented chip- and fiber-based architectures utilized for the generation, routing, and processing of various quantum photonic states encoded in the time domain (Roztocki et al., 2017; Reimer et al., 2015; Reimer et al., 2016; Reimer et al., 2019; Roztocki et al., 2021) provide compact, robust, and cost-effective schemes for the development of scalable technologies. The demonstrated higher-dimensional entanglement opens up promising avenues for utilizing time-bin encoded photon states in QKD, representing a competitive alternative to polarization- (Chen Y-A. et al., 2021; Takenaka et al., 2017; Sit et al., 2017), spatially- (Lo Franco and Compagno, 2018; Nosrati et al., 2020; Sun et al., 2020), and time- (Zhang et al., 2021) encoded counterparts for long-distance secure quantum communication applications. Additionally, to achieve transmission rates matching telecommunication standards and enable GHz speeds, multiplexing schemes with various independent sources (Pan et al., 2012) can be implemented.

Time-bin encoding has also been employed in hybrid quantum systems, combining the resilience of photonic states for long-distance transmission with the storage and processing capabilities of matter-based systems (Kimble, 2008; Sangouard et al., 2011). This approach has been successfully demonstrated in quantum dots, atomic ensembles, and nanophotonic systems (Appel et al., 2022; Yu et al., 2015; Farrera et al., 2018; Sun et al., 2022). Despite its potential, challenges remain, including managing photon indistinguishability, optimizing readout efficiencies, and mitigating noise from spin decoherence and multi-photon emissions. Advances such as magnetic field control to improve dephasing and coherence in atomic ensembles (Farrera et al., 2018) as well as optimized light-guiding technologies through photonic crystal waveguides for enhanced photon extraction efficiency (Appel et al., 2022) have significantly improved fidelity and scalability in entanglement generation and processing. Looking forward, time-bin hybrid encoding offers exciting possibilities for quantum repeaters and distributed quantum networks (Sun et al., 2022), with ongoing research aiming to optimize photon-matter interfaces and integrate diverse quantum systems into robust, scalable platforms.

In the field of quantum computation, the use of complex entangled photon states represents an important milestone for photonic platforms, although progress in this area has been limited. Tackling this, we reviewed an approach that was developed for time- and frequency-entangled quantum systems (Reimer et al., 2019), which can also be potentially extended to other degrees of freedom such as optical path (Rossi et al., 2009; Schaeff et al., 2012; Wang et al., 2018) and orbital angular momentum (Mair et al., 2001; Jennewein et al., 2000). Furthermore, the precise measurement of single-photon time differences relative to a reference pump laser is essential for dense information encoding and retrieval in time-bin quantum communication, while the time delay distribution between entangled photon detections is crucial for reconstructing biphoton wavefunctions. We review here a time-stretch sampling technique that significantly enhances the temporal resolution of single-photon detectors, improving the accuracy of time-correlated measurements. A notable advantage of the reported photonic schemes is the simplicity and ease of photon processing techniques enabled by off-the-shelf fiber-based components for quantum state measurements. The platforms discussed in this review represent a promising step towards the development of scalable, user-friendly, and affordable quantum photonic technologies for large-scale deployment on a global scale.

Author contributions

NM: Writing–original draft, Writing–review and editing. AG: Writing–review and editing. MM: Writing–review and editing. FN: Writing–review and editing. HY: Writing–review and editing. SS:

Writing–review and editing. BC: Writing–review and editing. UP: Writing–review and editing. ZW: Writing–review and editing. RL: Writing–review and editing. MC: Writing–review and editing. WM: Writing–review and editing. DM: Writing–review and editing. JA: Writing–review and editing. RM: Writing–review and editing.

Funding

The author(s) declare that financial support was received for the research and/or publication of this article. NM. and SS. acknowledge support from a Mitacs Elevate Thematic Postdoctoral Fellowship. MM. and UP. acknowledge support from Deutsche Forschungsgemeinschaft (DFG, German Research Foundation) – Project-ID 398816777 – SFB 1375 and Project-ID 259607349-GRK 2101. HY. acknowledges the financial support from the China Scholarship Council (CSC). BC. acknowledges NSERC for a Postgraduate Scholarship-Doctoral (PGS D). RLF. acknowledges support from MUR (Ministero dell'Università e della Ricerca) through the following projects: PNRR Project ICON-Q – Partenariato Esteso NQSTI – PE00000023 – Spoke 2 – CUP: J13C22000680006, PNRR Project QUANTIP – Partenariato Esteso NQSTI – PE00000023 – Spoke 9 – CUP: E63C22002180006, PNRR Project PRISM – Partenariato Esteso RESTART – PE00000001 – Spoke 4 – CUP: C79J24000190004. MC. acknowledges support from an NSERC (Natural Sciences and Engineering Council of Canada) Banting programme and from an FRQNT (Fonds de recherche du Québec – Nature et technologies) PBEEE (Bourses d'excellence pour étudiants (es) étrangers (ères)) programme. WJM. acknowledges partial support from the JSPS KAKENHI grant no. 21H04880. DJM. acknowledges funding support from the Australian Research Council Centre of Excellence COMBS (Centre for Optical Microcombs for Breakthrough Science), Project (No. CE230100006). JA. acknowledges support from NSERC and FRQNT. RM. acknowledges support from the Canada Research Chair Program, from the MEI i and from NSERC, through the following projects: AQUA ALLRP 587602-23, QuEnSi ALLRP 578468-22, Consortium on Integrated Quantum Photonics with Ferroelectric Materials ALLRP 587352-23, HyperSpace ALLRP 569583-21, and from FRQNT, through the project Ad.QuATS FRQNT 328872.

Conflict of interest

The authors declare that the research was conducted in the absence of any commercial or financial relationships that could be construed as a potential conflict of interest.

Generative AI statement

The author(s) declare that no Generative AI was used in the creation of this manuscript.

Publisher's note

All claims expressed in this article are solely those of the authors and do not necessarily represent those of their affiliated organizations, or those of the publisher, the editors and the reviewers. Any product that may be evaluated in this article, or claim that may be made by its manufacturer, is not guaranteed or endorsed by the publisher.

References

Alder, T., Stohr, A., Heinzelmann, R., and Jager, D. (2000). High-efficiency fiber-to-chip coupling using low-loss tapered single-mode fiber. *IEEE Photonics Technol. Lett.* 12 (8), 1016–1018. doi:10.1109/68.867993

Ali-Khan, I., Broadbent, C. J., and Howell, J. C. (2007). Large-alphabet quantum key distribution using energy-time entangled bipartite states. *Phys. Rev. Lett.* 98 (6), 060503. doi:10.1103/physrevlett.98.060503

Allgaier, M., Vigh, G., Ansari, V., Eigner, C., Quiring, V., Ricken, R., et al. (2017). Fast time-domain measurements on telecom single photons. *Quantum Sci. Technol.* 2 (3), 034012. doi:10.1088/2058-9565/aa7abb

Anderson, M., Müller, T., Skiba-Szymanska, J., Krysa, A., Huwer, J., Stevenson, R., et al. (2020). Gigahertz-clocked teleportation of time-bin qubits with a quantum dot in the telecommunication C band. *Phys. Rev. Appl.* 13 (5), 054052. doi:10.1103/physrevapplied.13.054052

Appas, F., Baboux, F., Amanti, M. I., Lemaítre, A., Boitier, F., Diamanti, E., et al. (2021). Flexible entanglement-distribution network with an AlGaAs chip for secure communications. *npj Quantum Inf.* 7 (1), 118. doi:10.1038/s41534-021-00454-7

Appel, M. H., Tiranov, A., Pabst, S., Chan, M. L., Starup, C., Wang, Y., et al. (2022). Entangling a hole spin with a time-bin photon: a waveguide approach for quantum dot sources of multiphoton entanglement. *Phys. Rev. Lett.* 128 (23), 233602. doi:10.1103/physrevlett.128.233602

Arrazola, J. M., Bergholm, V., Brádler, K., Bromley, T. R., Collins, M. J., Dhand, I., et al. (2021). Quantum circuits with many photons on a programmable nanophotonic chip. *Nature* 591 (7848), 54–60. doi:10.1038/s41586-021-03202-1

Barreiro, J. T., Wei, T.-C., and Kwiat, P. G. (2008). Beating the channel capacity limit for linear photonic superdense coding. *Nat. Phys.* 4 (4), 282–286. doi:10.1038/nphys919

Barwicz, T., Janta-Polczynski, A., Khater, M., Thibodeau, Y., Leidy, R., Maling, J., et al. (2015). "An O-band metamaterial converter interfacing standard optical fibers to silicon nanophotonic waveguides." In *Optical Fiber Communication Conference*. Optica Publishing Group, Th3F-3.

Bawankar, Y. R., and Singh, A. (2021). *Microring resonators based applications in silicon photonics-a review. 2021 5th conference on information and communication technology (CICT)* (IEEE).

Belthangady, C., Du, S., Chuu, C.-S., Yin, G., and Harris, S. E. (2009). Modulation and measurement of time-energy entangled photons. *Phys. Rev. A* 80 (3), 031803. doi:10.1103/physreva.80.031803

Benea-Chelmus, I.-C., Zhu, T., Settembrini, F. F., Bonzon, C., Mavrona, E., Elder, D. L., et al. (2018). Three-dimensional phase modulator at telecom wavelength acting as a terahertz detector with an electro-optic bandwidth of 1.25 terahertz. *ACS Photonics* 5 (4), 1398–1403. doi:10.1021/acsphotonics.7b01407

Bernien, H., Schwartz, S., Keesling, A., Levine, H., Omran, A., Pichler, H., et al. (2017). Probing many-body dynamics on a 51-atom quantum simulator. *Nature* 551 (7682), 579–584. doi:10.1038/nature24622

Blumenthal, D. J. (2020). Photonic integration for UV to IR applications. *APL Photonics* 5 (2), 020903. doi:10.1063/1.5131683

Boaron, A., Boso, G., Rusca, D., Vulliez, C., Autebert, C., Caloz, M., et al. (2018). Secure quantum key distribution over 421 km of optical fiber. *Phys. Rev. Lett.* 121 (19), 190502. doi:10.1103/physrevlett.121.190502

Bonneau, D., Silverstone, J. W., and Thompson, M. G. (2016). Silicon quantum photonics. *Top. Appl. Phys.*, 41–82. doi:10.1007/978-3-642-10503-6_2

Bouchard, F., Bonsma-Fisher, K., Heshami, K., Bustard, P. J., England, D., and Sussman, B. (2023). Measuring ultrafast time-bin qudits. *Phys. Rev. A* 107 (2), 022618. doi:10.1103/physreva.107.022618

Bourassa, J. E., Alexander, R. N., Vasmer, M., Patil, A., Tzitrin, I., Matsuura, T., et al. (2021). Blueprint for a scalable photonic fault-tolerant quantum computer. *Quantum* 5, 392. doi:10.22331/q-2021-02-04-392

Brendel, J., Gisin, N., Tittel, W., and Zbinden, H. (1999). Pulsed energy-time entangled twin-photon source for quantum communication. *Phys. Rev. Lett.* 82 (12), 2594–2597. doi:10.1103/physrevlett.82.2594

Briegel, H. J., and Raussendorf, R. (2001). Persistent entanglement in arrays of interacting particles. *Phys. Rev. Lett.* 86 (5), 910–913. doi:10.1103/physrevlett.86.910

Bromley, T. R., Arrazola, J. M., Jahangiri, S., Izaac, J., Quesada, N., Gran, A. D., et al. (2020). Applications of near-term photonic quantum computers: software and algorithms. *Quantum Sci. Technol.* 5 (3), 034010. doi:10.1088/2058-9565/ab8504

Brown, R. H., and Twiss, R. Q. (1956). Correlation between photons in two coherent beams of light. *Nature* 177 (4497), 27–29. doi:10.1038/177027a0

Bruschini, C., Homulle, H., Antolovic, I. M., Burri, S., and Charbon, E. (2019). Single-photon avalanche diode imagers in biophotonics: review and outlook. *Light Sci. and Appl.* 8 (1), 87. doi:10.1038/s41377-019-0191-5

Burla, M., Hoessbacher, C., Heni, W., Haffner, C., Fedoryshyn, Y., Werner, D., et al. (2019). 500 GHz plasmonic Mach-Zehnder modulator enabling sub-THz microwave photonics. *APL Photonics* 4 (5). doi:10.1063/1.5086868

Burlakov, A., Chekhova, M., Karabutova, O., and Kulik, S. (2001). Collinear two-photon state with spectral properties of type-I and polarization properties of type-II spontaneous parametric down-conversion: preparation and testing. *Phys. Rev. A* 64 (4), 041803. doi:10.1103/physreva.64.041803

Cabello, A., Rossi, A., Vallone, G., De Martini, F., and Mataloni, P. (2009). Proposed Bell experiment with genuine energy-time entanglement. *Phys. Rev. Lett.* 102 (4), 040401. doi:10.1103/physrevlett.102.040401

Carvacho, G., Carine, J., Saavedra, G., Cuevas, Á., Fuenzalida, J., Toledo, F., et al. (2015). Postselection-loophole-free Bell test over an installed optical fiber network. *Phys. Rev. Lett.* 115 (3), 030503. doi:10.1103/physrevlett.115.030503

Caspani, L., Reimer, C., Kues, M., Roztocki, P., Clerici, M., Wetzel, B., et al. (2016). Multifrequency sources of quantum correlated photon pairs on-chip: a path toward integrated Quantum Frequency Combs. *Nanophotonics* 5 (2), 351–362. doi:10.1515/nanoph-2016-0029

Caspani, L., Xiong, C., Eggleton, B. J., Bajoni, D., Liscidini, M., Galli, M., et al. (2017). Integrated sources of photon quantum states based on nonlinear optics. *Light Sci. and Appl.* 6 (11), e17100–e. doi:10.1038/lsa.2017.100

Chapman, J. C., Lim, C. C., and Kwiat, P. G. (2022). Hyperentangled time-bin and polarization quantum key distribution. *Phys. Rev. Appl.* 18 (4), 044027. doi:10.1103/physrevapplied.18.044027

Cheben, P., Bock, P. J., Schmid, J. H., Lapointe, J., Janz, S., Xu, D.-X., et al. (2010). Refractive index engineering with subwavelength gratings for efficient microphotonic couplers and planar waveguide multiplexers. *Opt. Lett.* 35 (15), 2526–2528. doi:10.1364/ol.35.002526

Cheben, P., Schmid, J. H., Wang, S., Xu, D.-X., Vachon, M., Janz, S., et al. (2015). Broadband polarization independent nanophotonic coupler for silicon waveguides with ultra-high efficiency. *Opt. express* 23 (17), 22553–22563. doi:10.1364/oe.23.022553

Chen, C., Xu, C., Riazi, A., Zhu, E. Y., Gladyshev, A. V., Kazansky, P. G., et al. (2021a). Broadband fiber-based entangled photon-pair source at telecom O-band. *Opt. Lett.* 46 (6), 1261–1264. doi:10.1364/ol.415409

Chen, C., Xu, C., Riazi, A., Zhu, E. Y., Greenwood, A. C., Gladyshev, A. V., et al. (2022). Telecom-band hyperentangled photon pairs from a fiber-based source. *Phys. Rev. A* 105 (4), 043702. doi:10.1103/physreva.105.043702

Chen, K., Li, C.-M., Zhang, Q., Chen, Y.-A., Goebel, A., Chen, S., et al. (2007). Experimental realization of one-way quantum computing with two-photon four-qubit cluster states. *Phys. Rev. Lett.* 99 (12), 120503. doi:10.1103/physrevlett.99.120503

Chen, Y.-A., Zhang, Q., Chen, T.-Y., Cai, W.-Q., Liao, S.-K., Zhang, J., et al. (2021b). An integrated space-to-ground quantum communication network over 4,600 kilometres. *Nature* 589 (7841), 214–219. doi:10.1038/s41586-020-03093-8

Chen, Z., and Segev, M. (2021). Highlighting photonics: looking into the next decade. *ELight* 1 (1), 2. doi:10.1186/s43593-021-00002-y

Chi, Y., Huang, J., Zhang, Z., Mao, J., Zhou, Z., Chen, X., et al. (2022). A programmable qudit-based quantum processor. *Nat. Commun.* 13 (1), 1166. doi:10.1038/s41467-022-28767-x

Cho, S.-B., and Noh, T.-G. (2009). Stabilization of a long-armed fiber-optic single-photon interferometer. *Opt. Express* 17 (21), 19027–19032. doi:10.1364/oe.17.019027

Ciampini, M. A., Orieux, A., Paesani, S., Sciarrino, F., Corrielli, G., Crespi, A., et al. (2016). Path-polarization hyperentangled and cluster states of photons on a chip. *Light Sci. and Appl.* 5 (4), e16064–e. doi:10.1038/lsa.2016.64

Clementi, M., Sabattoli, F. A., Borghi, M., Gianini, L., Tagliavacche, N., El Dirani, H., et al. (2023). Programmable frequency-bin quantum states in a nano-engineered silicon device. *Nat. Commun.* 14 (1), 176–210. doi:10.1038/s41467-022-35773-6

Cleve, R., Gottesman, D., and Lo, H.-K. (1999). How to share a quantum secret. *Phys. Rev. Lett.* 83 (3), 648–651. doi:10.1103/physrevlett.83.648

Collins, D., Gisin, N., Linden, N., Massar, S., and Popescu, S. (2002). Bell inequalities for arbitrarily high-dimensional systems. *Phys. Rev. Lett.* 88 (4), 040404. doi:10.1103/physrevlett.88.040404

Cozzolino, D., Da Lio, B., Bacco, D., and Oxenløwe, L. K. (2019). High-dimensional quantum communication: benefits, progress, and future challenges. *Adv. Quantum Technol.* 2 (12), 1900038. doi:10.1002/qute.201900038

Crockett, B., van Howe, J., Montaut, N., Morandotti, R., and Azaña, J. (2022). High-resolution time-correlated single-photon counting using electro-optic sampling. *Laser and Photonics Rev.* 16 (10), 2100635. doi:10.1002/lpor.202100635

Cuevas, A., Carvacho, G., Saavedra, G., Cariñe, J., Nogueira, W., Figueroa, M., et al. (2013). Long-distance distribution of genuine energy-time entanglement. *Nat. Commun.* 4 (1), 2871. doi:10.1038/ncomms3871

Dayan, B., Pe'Er, A., Friesem, A. A., and Silberberg, Y. (2004). Two photon absorption and coherent control with broadband down-converted light. *Phys. Rev. Lett.* 93 (2), 023005. doi:10.1103/physrevlett.93.023005

Debnath, S., Linke, N. M., Figgatt, C., Landsman, K. A., Wright, K., and Monroe, C. (2016). Demonstration of a small programmable quantum computer with atomic qubits. *Nature* 536 (7614), 63–66. doi:10.1038/nature18648

De Riedmatten, H., Marcikic, I., Scarani, V., Tittel, W., Zbinden, H., and Gisin, N. (2004). Tailoring photonic entanglement in high-dimensional Hilbert spaces. *Phys. Rev. A* 69 (5), 050304. doi:10.1103/physreva.69.050304

Dixon, A., Yuan, Z., Dynes, J., Sharpe, A., and Shields, A. (2008). Gigahertz decoy quantum key distribution with 1 Mbit/s secure key rate. *Opt. Express* 16 (23), 18790–18797. doi:10.1364/oe.16.018790

Donohue, J. , Mastrovich, M., and Resch, K. (2016). Spectrally engineering photonic entanglement with a time lens. *Phys. Rev. Lett.* 117 (24), 243602. doi:10.1103/physrevlett.117.243602

Eberhard, P. H. (1993). Background level and counter efficiencies required for a loophole-free Einstein-Podolsky-Rosen experiment. *Phys. Rev. A* 47 (2), R747–R750. doi:10.1103/physreva.47.r747

Ecker, S., Bouchard, F., Bulla, L., Brandt, F., Kohout, O., Steinlechner, F., et al. (2019). Overcoming noise in entanglement distribution. *Phys. Rev. X* 9 (4), 041042. doi:10.1103/physrevx.9.041042

Elshaari, A. W., Pernice, W., Srinivasan, K., Benson, O., and Zwiller, V. (2020). Hybrid integrated quantum photonic circuits. *Nat. Photonics* 14 (5), 285–298. doi:10.1038/s41566-020-0609-x

Fang, W.-T., Li, Y.-H., Zhou, Z.-Y., Xu, L.-X., Guo, G.-C., and Shi, B.-S. (2018). On-chip generation of time-and wavelength-division multiplexed multiple time-bin entanglement. *Opt. Express* 26 (10), 12912–12921. doi:10.1364/oe.26.012912

Farrera, P., Heinze, G., and De Riedmatten, H. (2018). Entanglement between a photonic time-bin qubit and a collective atomic spin excitation. *Phys. Rev. Lett.* 120 (10), 100501. doi:10.1103/physrevlett.120.100501

Faruque, I. I., Sinclair, G. F., Bonneau, D., Rarity, J. G., and Thompson, M. G. (2018). On-chip quantum interference with heralded photons from two independent micro-ring resonator sources in silicon photonics. *Opt. Express* 26 (16), 20379–20395. doi:10.1364/oe.26.020379

Finco, G., Miserocchi, F., Maeder, A., Kellner, J., Sabatti, A., Chapman, R. J., et al. (2024). Time-bin entangled Bell state generation and tomography on thin-film lithium niobate. *Quantum Inf.* 10, 135. doi:10.1038/s41534-024-00925-7

Fitzke, E., Bialowons, L., Dolejsky, T., Tippmann, M., Nikiforov, O., Walther, T., et al. (2022). Scalable network for simultaneous pairwise quantum key distribution via entanglement-based time-bin coding. *PRX Quantum* 3 (2), 020341. doi:10.1103/prxquantum.3.020341

Flamini, F., Spagnolo, N., and Sciarrino, F. (2018). Photonic quantum information processing: a review. *Rep. Prog. Phys.* 82 (1), 016001. doi:10.1088/1361-6633/aad5b2

Franson, J. (1992). Nonlocal cancellation of dispersion. *Phys. Rev. A* 45 (5), 3126–3132. doi:10.1103/physreva.45.3126

Franson, J. D. (1989). Bell inequality for position and time. *Phys. Rev. Lett.* 62 (19), 2205–2208. doi:10.1103/physrevlett.62.2205

Friberg, S., Hong, C., and Mandel, L. (1985). Measurement of time delays in the parametric production of photon pairs. *Phys. Rev. Lett.* 54 (18), 2011–2013. doi:10.1103/physrevlett.54.2011

Frigg, A., Boes, A., Ren, G., Abdo, I., Choi, D.-Y., Gees, S., et al. (2019). Low loss CMOS-compatible silicon nitride photonics utilizing reactive sputtered thin films. *Opt. Express* 27 (26), 37795–37805. doi:10.1364/oe.380758

Gariepy, G., Krstajić, N., Henderson, R., Li, C., Thomson, R. R., Buller, G. S., et al. (2015). Single-photon sensitive light-in-fight imaging. *Nat. Commun.* 6 (1), 6021. doi:10.1038/ncomms7021

Giovannetti, V., Lloyd, S., and Maccone, L. (2011). Advances in quantum metrology. *Nat. Photonics* 5 (4), 222–229. doi:10.1038/nphoton.2011.35

Goldschmidt, E. A., Eisaman, M. D., Fan, J., Polyakov, S. V., and Migdall, A. (2008). Spectrally bright and broad fiber-based heralded single-photon source. *Phys. Rev. A* 78 (1), 013844. doi:10.1103/physreva.78.013844

Grassani, D., Simbula, A., Pirotta, S., Galli, M., Menotti, M., Harris, N. C., et al. (2016). Energy correlations of photon pairs generated by a silicon microring resonator probed by Stimulated Four Wave Mixing. *Sci. Rep.* 6 (1), 23564. doi:10.1038/srep23564

Harris, S. (2008). Nonlocal modulation of entangled photons. *Phys. Rev. A* 78 (2), 021807. doi:10.1103/physreva.78.021807

Harris, S., Oshman, M., and Byer, R. (1967). Observation of tunable optical parametric fluorescence. *Phys. Rev. Lett.* 18 (18), 732–734. doi:10.1103/physrevlett.18.732

Harrow, A. W., and Montanaro, A. (2017). Quantum computational supremacy. *Nature* 549 (7671), 203–209. doi:10.1038/nature23458

He, L., Zhang, M., Shams-Ansari, A., Zhu, R., Wang, C., and Marko, L. (2019). Low-loss fiber-to-chip interface for lithium niobate photonic integrated circuits. *Opt. Lett.* 44 (9), 2314–2317. doi:10.1364/ol.44.002314

Helt, L. G., Yang, Z., Liscidini, M., and Sipe, J. E. (2010). Spontaneous four-wave mixing in microring resonators. *Opt. Lett.* 35 (18), 3006–3008. doi:10.1364/ol.35.003006

Henriet, L., Beguin, L., Signoles, A., Lahaye, T., Browaeys, A., Reymond, G.-O., et al. (2020). Quantum computing with neutral atoms. *Quantum* 4, 327. doi:10.22331/q-2020-09-21-327

Heuck, M., Koefoed, J. G., Christensen, J. B., Ding, Y., Frandsen, L. H., Rottwitt, K., et al. (2019). Unidirectional frequency conversion in microring resonators for on-chip frequency-multiplexed single-photon sources. *New J. Phys.* 21 (3), 033037. doi:10.1088/1367-2630/ab09a7

Hillery, M., Bužek, V., and Berthiaume, A. (1999). Quantum secret sharing. *Phys. Rev. A* 59 (3), 1829–1834. doi:10.1103/physreva.59.1829

Horodecki, M., Horodecki, P., and Horodecki, R. (1996). Separability of mixed quantum states: necessary and sufficient conditions. *Phys. Lett.* doi:10.1016/s0375-9601(96)00706-2

Huang, J., Chi, Y., Zhang, Z., Yang, Y., Gong, Q., and Wang, J. (2022). "A programmable photonic chip for high-dimensional quantum computing," *TENCON 2022-2022 IEEE region 10 conference (TENCON)* (IEEE).

Humphreys, P. C., Metcalf, B. J., Spring, J. B., Moore, M., Jin, X.-M., Barbieri, M., et al. (2013). Linear optical quantum computing in a single spatial mode. *Phys. Rev. Lett.* 111 (15), 150501. doi:10.1103/physrevlett.111.150501

Hunault, M., Takesue, H., Tadanaga, O., Nishida, Y., and Asobe, M. (2010). Generation of time-bin entangled photon pairs by cascaded second-order nonlinearity in a single periodically poled LiNbO_3 waveguide. *Opt. Lett.* 35 (8), 1239–1241. doi:10.1364/ol.35.001239

Ikuta, T., and Takesue, H. (2018). Four-dimensional entanglement distribution over 100 km. *Sci. Rep.* 8 (1), 817. doi:10.1038/s41598-017-19078-z

Imany, P., Jaramillo-Villegas, J. A., Odele, O. D., Han, K., Leaird, D. E., Lukens, J. M., et al. (2018). 50-GHz-spaced comb of high-dimensional frequency-bin entangled photons from an on-chip silicon nitride microresonator. *Opt. Express* 26 (2), 1825–1840. doi:10.1364/oe.26.001825

Islam, N. T., Lim, C. C. W., Cahall, C., Kim, J., and Gauthier, D. J. (2017). Provably secure and high-rate quantum key distribution with time-bin qudits. *Sci. Adv.* 3 (11), e1701491. doi:10.1126/sciadv.1701491

Israel, Y., Rosen, S., and Silberberg, Y. (2014). Supersensitive polarization microscopy using NOON states of light. *Phys. Rev. Lett.* 112 (10), 103604. doi:10.1103/physrevlett.112.103604

Jayakody, M. N., Pradhan, P., Ben Porath, D., and Cohen, E. (2023). Discrete-time quantum walk on multilayer networks. *Entropy* 25 (12), 1610. doi:10.3390/e25121610

Jennewein, T., Simon, C., Weihs, G., Weinfurter, H., and Zeilinger, A. (2000). Quantum cryptography with entangled photons. *Phys. Rev. Lett.* 84 (20), 4729–4732. doi:10.1103/physrevlett.84.4729

Jin, H., Liu, F., Xu, P., Xia, J., Zhong, M., Yuan, Y., et al. (2014). On-chip generation and manipulation of entangled photons based on reconfigurable lithium-niobate waveguide circuits. *Phys. Rev. Lett.* 113 (10), 103601. doi:10.1103/physrevlett.113.103601

Jin, J., Bourgoin, J.-P., Tannous, R., Agne, S., Pugh, C. J., Kuntz, K. B., et al. (2019). Genuine time-bin-encoded quantum key distribution over a turbulent depolarizing free-space channel. *Opt. Express* 27 (26), 37214–37223. doi:10.1364/oe.27.037214

Kanada, T., and Franzen, D. L. (1986). Optical waveform measurement by optical sampling with a mode-locked laser diode. *Opt. Lett.* 11 (1), 4–6. doi:10.1364/ol.11.000004

Kaneda, F., Christensen, B. G., Wong, J. J., Park, H. S., McCusker, K. T., and Kwiat, P. G. (2015). Time-multiplexed heralded single-photon source. *Optica* 2 (12), 1010–1013. doi:10.1364/optica.2.001010

Kasaya, K., Mitomi, O., Naganuma, M., Kondo, Y., and Noguchi, Y. (1993). A simple laterally tapered waveguide for low-loss coupling to single-mode fibers. *IEEE Photonics Technol. Lett.* 5 (3), 345–347. doi:10.1109/68.205633

Kharel, P., Reimer, C., Luke, K., He, L., and Zhang, M. (2021). Breaking voltage–bandwidth limits in integrated lithium niobate modulators using micro-structured electrodes. *Optica* 8 (3), 357–363. doi:10.1364/optica.416155

Kiesel, N., Schmid, C., Weber, U., Tóth, G., Gühne, O., Ursin, R., et al. (2005). Experimental analysis of a four-qubit photon cluster state. *Phys. Rev. Lett.* 95 (21), 210502. doi:10.1103/physrevlett.95.210502

Kim, Y.-H., Kulik, S. P., and Shih, Y. (2001). Quantum teleportation of a polarization state with a complete Bell state measurement. *Phys. Rev. Lett.* 86 (7), 1370–1373. doi:10.1103/physrevlett.86.1370

Kimble, H. J. (2008). The quantum internet. *Nature* 453 (7198), 1023–1030. doi:10.1038/nature07127

Kitaev, A. Y. (1995). Quantum measurements and the Abelian stabilizer problem. Available online at: https://arxiv.org/abs/quant-ph/9511026. (Accessed March 24, 2025).

Knill, E., Laflamme, R., and Milburn, G. J. (2001). A scheme for efficient quantum computation with linear optics. *Nature* 409 (6816), 46–52. doi:10.1038/35051009

Knips, L., Schwemmer, C., Klein, N., Wieśniak, M., and Weinfurter, H. (2016). Multipartite entanglement detection with minimal effort. *Phys. Rev. Lett.* 117 (21), 210504. doi:10.1103/physrevlett.117.210504

Korzh, B., Lim, C. C. W., Houlmann, R., Gisin, N., Li, M. J., Nolan, D., et al. (2015). Provably secure and practical quantum key distribution over 307 km of optical fibre. *Nat. Photonics* 9 (3), 163–168. doi:10.1038/nphoton.2014.327

Krenn, M., Handsteiner, J., Fink, M., Fickler, R., Ursin, R., Malik, M., et al. (2016b). Twisted light transmission over 143 km. *Proc. Natl. Acad. Sci.* 113 (48), 13648–13653. doi:10.1073/pnas.1612023113

Krenn, M., Malik, M., Scheidl, T., Ursin, R., and Zeilinger, A. (2016a). Quantum communication with photons. *Opt. Our Time* 18, 455–482. doi:10.1007/978-3-319-31903-2_18

Kues, M., Reimer, C., Roztocki, P., Cortés, L. R., Sciara, S., Wetzel, B., et al. (2017). On-chip generation of high-dimensional entangled quantum states and their coherent control. *Nature* 546 (7660), 622–626. doi:10.1038/nature22986

Kultavewuti, P., Zhu, E. Y., Xing, X., Qian, L., Pusino, V., Sorel, M., et al. (2017). Polarization-entangled photon pair sources based on spontaneous four wave mixing assisted by polarization mode dispersion. *Sci. Rep.* 7 (1), 5785. doi:10.1038/s41598-017-06010-8

Kuzucu, O., Wong, F. N., Kurimura, S., and Tovstonog, S. (2008). Time-resolved single-photon detection by femtosecond upconversion. *Opt. Lett.* 33 (19), 2257–2259. doi:10.1364/ol.33.002257

Kwiat, P. G. (1997). Hyper-entangled states. *J. Mod. Opt.* 44 (11-12), 2173–2184. doi:10.1080/09500349708231877

Kwiat, P. G., Waks, E., White, A. G., Appelbaum, I., and Eberhard, P. H. (1999). Ultrabright source of polarization-entangled photons. *Phys. Rev. A* 60 (2), R773–R776. doi:10.1103/physreva.60.r773

Kwon, O., Ra, Y.-S., and Kim, Y.-H. (2009). Coherence properties of spontaneous parametric down-conversion pumped by a multi-mode cw diode laser. *Opt. Express* 17 (15), 13059–13069. doi:10.1364/oe.17.013059

Leifgen, M., Schröder, T., Gädeke, F., Riemann, R., Métillon, V., Neu, E., et al. (2014). Evaluation of nitrogen-and silicon-vacancy defect centres as single photon sources in quantum key distribution. *New J. Phys.* 16 (2), 023021. doi:10.1088/1367-2630/16/2/023021

Li, Q., Davanço, M., and Srinivasan, K. (2016). Efficient and low-noise single-photon-level frequency conversion interfaces using silicon nanophotonics. *Nat. Photonics* 10 (6), 406–414. doi:10.1038/nphoton.2016.64

Liao, S.-K., Yong, H.-L., Liu, C., Shentu, G.-L., Li, D.-D., Lin, J., et al. (2017). Long-distance free-space quantum key distribution in daylight towards inter-satellite communication. *Nat. Photonics* 11 (8), 509–513. doi:10.1038/nphoton.2017.116

Lima, G., Vallone, G., Chiuri, A., Cabello, A., and Mataloni, P. (2010). Experimental Bell-inequality violation without the postselection loophole. *Phys. Rev. A* 81 (4), 040101. doi:10.1103/physreva.81.040101

Liu, X., Kuyken, B., Roelkens, G., Baets, R., Osgood, R. M., Jr, and Green, W. M. (2012). Bridging the mid-infrared-to-telecom gap with silicon nanophotonic spectral translation. *Nat. Photonics* 6 (10), 667–671. doi:10.1038/nphoton.2012.221

Llewellyn, D., Ding, Y., Faruque, I. I., Paesani, S., Bacco, D., Santagati, R., et al. (2020). Chip-to-chip quantum teleportation and multi-photon entanglement in silicon. *Nat. Phys.* 16 (2), 148–153. doi:10.1038/s41567-019-0727-x

Lo, H.-K., Curty, M., and Tamaki, K. (2014). Secure quantum key distribution. *Nat. Photonics* 8 (8), 595–604. doi:10.1038/nphoton.2014.149

Lo Franco, R., and Compagno, G. (2018). Indistinguishability of elementary systems as a resource for quantum information processing. *Phys. Rev. Lett.* 120 (24), 240403. doi:10.1103/physrevlett.120.240403

Lovett, N. B., Cooper, S., Everitt, M., Trevers, M., and Kendon, V. (2010). Universal quantum computation using the discrete-time quantum walk. *Phys. Rev. A* 81 (4), 042330. doi:10.1103/physreva.81.042330

Lu, H.-H., Lukens, J. M., Peters, N. A., Williams, B. P., Weiner, A. M., and Lougovski, P. (2018). Quantum interference and correlation control of frequency-bin qubits. *Optica* 5 (11), 1455–1460. doi:10.1364/optica.5.001455

Lu, L., Zheng, X., Lu, Y., Zhu, S., and Ma, X. S. (2021). Advances in chip-scale quantum photonic technologies. *Adv. Quantum Technol.* 4 (12), 2100068. doi:10.1002/qute.202100068

Lu, X., Li, Q., Westly, D. A., Moille, G., Singh, A., Anant, V., et al. (2019). Chip-integrated visible–telecom entangled photon pair source for quantum communication. *Nat. Phys.* 15 (4), 373–381. doi:10.1038/s41567-018-0394-3

Lukens, J. M., Odele, O., Langrock, C., Fejer, M. M., Leaird, D. E., and Weiner, A. M. (2014). Generation of biphoton correlation trains through spectral filtering. *Opt. Express* 22 (8), 9585–9596. doi:10.1364/oe.22.009585

Lukens, J. M., Odele, O. D., Leaird, D. E., and Weiner, A. M. (2015). Electro-optic modulation for high-speed characterization of entangled photon pairs. *Opt. Lett.* 40 (22), 5331–5334. doi:10.1364/ol.40.005331

Luo, Y.-H., Zhong, H.-S., Erhard, M., Wang, X.-L., Peng, L.-C., Krenn, M., et al. (2019). Quantum teleportation in high dimensions. *Phys. Rev. Lett.* 123 (7), 070505. doi:10.1103/physrevlett.123.070505

Lv, N., Zhang, W., Guo, Y., Zhou, Q., Huang, Y., and Peng, J. (2013). 1.5 μm polarization entanglement generation based on birefringence in silicon wire waveguides. *Opt. Lett.* 38 (15), 2873–2876. doi:10.1364/ol.38.002873

Ma, X.-S., Herbst, T., Scheidl, T., Wang, D., Kropatschek, S., Naylor, W., et al. (2012). Quantum teleportation over 143 kilometres using active feed-forward. *Nature* 489 (7415), 269–273. doi:10.1038/nature11472

MacLean, J.-P. W., Donohue, J. M., and Resch, K. J. (2018a). Ultrafast quantum interferometry with energy-time entangled photons. *Phys. Rev. A* 97 (6), 063826. doi:10.1103/physreva.97.063826

MacLean, J.-P. W., Donohue, J. M., and Resch, K. J. (2018b). Direct characterization of ultrafast energy-time entangled photon pairs. *Phys. Rev. Lett.* 120 (5), 053601. doi:10.1103/physrevlett.120.053601

Magde, D., and Mahr, H. (1967). Study in ammonium dihydrogen phosphate of spontaneous parametric interaction tunable from 4400 to 16 000 Å. *Phys. Rev. Lett.* 18 (21), 905–907. doi:10.1103/physrevlett.18.905

Mair, A., Vaziri, A., Weihs, G., and Zeilinger, A. (2001). Entanglement of the orbital angular momentum states of photons. *Nature* 412 (6844), 313–316. doi:10.1038/35085529

Marcikic, I., de Riedmatten, H., Tittel, W., Scarani, V., Zbinden, H., and Gisin, N. (2002). Femtosecond time-bin entangled qubits for quantum communication. arXiv preprint quant-ph/0205144.

Marcikic, I., De Riedmatten, H., Tittel, W., Zbinden, H., Legré, M., and Gisin, N. (2004). Distribution of time-bin entangled qubits over 50 km of optical fiber. *Phys. Rev. Lett.* 93 (18), 180502. doi:10.1103/physrevlett.93.180502

Martin, H., and Jiang, X. (2010). Rapid phase-shifting fiber interferometer with optical stylus. *Opt. Lett.* 35 (5), 655–657. doi:10.1364/ol.35.000655

Masters, B. R. (2014). *Fluorescence lifetime spectroscopy and imaging: principles and applications in biomedical diagnostics.* 109901.

Matthews, J. C., Zhou, X.-Q., Cable, H., Shadbolt, P. J., Saunders, D. J., Durkin, G. A., et al. (2016). Towards practical quantum metrology with photon counting. *npj Quantum Inf.* 2 (1), 16023–16027. doi:10.1038/npjqi.2016.23

Metcalf, B. J., Spring, J. B., Humphreys, P. C., Thomas-Peter, N., Barbieri, M., Kolthammer, W. S., et al. (2014). Quantum teleportation on a photonic chip. *Nat. Photonics* 8 (10), 770–774. doi:10.1038/nphoton.2014.217

Miller, D., Holz, T., Kampermann, H., and Bruß, D. (2018). Propagation of generalized pauli errors in qudit clifford circuits. *Phys. Rev. A* 98 (5), 052316. doi:10.1103/physreva.98.052316

Mittal, S., Orre, V. V., Restelli, A., Salem, R., Goldschmidt, E. A., and Hafezi, M. (2017). Temporal and spectral manipulations of correlated photons using a time lens. *Phys. Rev. A* 96 (4), 043807. doi:10.1103/physreva.96.043807

Monika, M., Nosrati, F., George, A., Sciara, S., Fazili, R., Marques Muniz, A. L., et al. (2024). Quantum state processing through controllable synthetic temporal photonic lattices. *Nat. Photonics* 19, 95–100. doi:10.1038/s41566-024-01546-4

Montaut, N., Sansoni, L., Meyer-Scott, E., Ricken, R., Quiring, V., Herrmann, H., et al. (2017). High-efficiency plug-and-play source of heralded single photons. *Phys. Rev. Appl.* 8 (2), 024021. doi:10.1103/physrevapplied.8.024021

Moody, G., Sorger, V. J., Blumenthal, D. J., Juodawlkis, P. W., Loh, W., Sorace-Agaskar, C., et al. (2022). 2022 Roadmap on integrated quantum photonics. *J. Phys. Photonics* 4 (1), 012501. doi:10.1088/2515-7647/ac1ef4

Mooney, G. J., Hill, C. D., and Hollenberg, L. C. (2019). Entanglement in a 20-qubit superconducting quantum computer. *Sci. Rep.* 9 (1), 13465. doi:10.1038/s41598-019-49805-7

Mueller, A., Davis, S. I., Korzh, B., Valivarthi, R., Beyer, A. D., Youssef, R., et al. (2024). High-rate multiplexed entanglement source based on time-bin qubits for advanced quantum networks. *Opt. Quantum* 2 (2), 64–71. doi:10.1364/opticaq.509335

Musiał, A., Żołnacz, K., Srocka, N., Kravets, O., Große, J., Olszewski, J., et al. (2020). Plug&play fiber-coupled 73 kHz single-photon source operating in the telecom o-band. *Adv. Quantum Technol.* 3 (6), 2000018. doi:10.1002/qute.202000018

Niffenegger, R. J., Stuart, J., Sorace-Agaskar, C., Kharas, D., Bramhavar, S., Bruzewicz, C. D., et al. (2020). Integrated multi-wavelength control of an ion qubit. *Nature* 586 (7830), 538–542. doi:10.1038/s41586-020-2811-x

Nikles, M., Thévenaz, L., Robert, P. A., and von der Weid, J. P. (1995). Optical sampling using wideband electro-optic modulators. *Opt. Eng.* 34 (7), 2078–2083. doi:10.1117/12.204801

Noda, J., Mikami, O., Minakata, M., and Fukuma, M. (1978). Single-mode optical-waveguide fiber coupler. *Appl. Opt.* 17 (13), 2092–2096. doi:10.1364/ao.17.002092

Nosrati, F., Castellini, A., Compagno, G., and Lo Franco, R. (2020). Robust entanglement preparation against noise by controlling spatial indistinguishability. *npj Quantum Inf.* 6 (1), 39. doi:10.1038/s41534-020-0271-7

Olislager, L., Cussey, J., Nguyen, A. T., Emplit, P., Massar, S., Merolla, J.-M., et al. (2010). Frequency-bin entangled photons. *Phys. Rev. A* 82 (1), 013804. doi:10.1103/physreva.82.013804

Ono, T., Tsujimoto, Y., Wakui, K., and Fujiwara, M. (2024). Quantum interference of pulsed time-bin entanglement generated from silicon ring resonator. *Sci. Rep.* 14 (1), 1051. doi:10.1038/s41598-024-51311-4

Pan, J.-W., Chen, Z.-B., Lu, C.-Y., Weinfurter, H., Zeilinger, A., and Żukowski, M. (2012). Multiphoton entanglement and interferometry. *Rev. Mod. Phys.* 84 (2), 777–838. doi:10.1103/revmodphys.84.777

Pasquazi, A., Peccianti, M., Razzari, L., Moss, D. J., Coen, S., Erkintalo, M., et al. (2018). Micro-combs: a novel generation of optical sources. *Phys. Rep.* 729, 1–81. doi:10.1016/j.physrep.2017.08.004

Pelucchi, E., Fagas, G., Aharonovich, I., Englund, D., Figueroa, E., Gong, Q., et al. (2021). The potential and global outlook of integrated photonics for quantum technologies. *Nat. Rev. Phys.* 4 (3), 194–208. doi:10.1038/s42254-021-00398-z

Pirandola, S., Bardhan, B. R., Gehring, T., Weedbrook, C., and Lloyd, S. (2018). Advances in photonic quantum sensing. *Nat. Photonics* 12 (12), 724–733. doi:10.1038/s41566-018-0301-6

Pirandola, S., Eisert, J., Weedbrook, C., Furusawa, A., and Braunstein, S. L. (2015). Advances in quantum teleportation. *Nat. Photonics* 9 (10), 641–652. doi:10.1038/nphoton.2015.154

Prevedel, R., Walther, P., Tiefenbacher, F., Böhi, P., Kaltenbaek, R., Jennewein, T., et al. (2007). High-speed linear optics quantum computing using active feed-forward. *Nature* 445 (7123), 65–69. doi:10.1038/nature05346

Pulford, D., Robillard, C., and Huntington, E. (2005). Single photon locking of an all-fiber interferometer. *Rev. Sci. Instrum.* 76 (6), 063114. doi:10.1063/1.1922327

Rapp, J., Dawson, R. M., and Goyal, V. K. (2020). Dithered depth imaging. *Opt. Express* 28 (23), 35143–35157. doi:10.1364/oe.408800

Raussendorf, R., and Briegel, H. J. (2001). A one-way quantum computer. *Phys. Rev. Lett.* 86 (22), 5188–5191. doi:10.1103/physrevlett.86.5188

Regensburger, A., Bersch, C., Miri, M.-A., Onishchukov, G., Christodoulides, D. N., and Peschel, U. (2012). Parity–time synthetic photonic lattices. *Nature* 488 (7410), 167–171. doi:10.1038/nature11298

Rehain, P., Sua, Y. M., Zhu, S., Dickson, I., Muthuswamy, B., Ramanathan, J., et al. (2020). Noise-tolerant single photon sensitive three-dimensional imager. *Nat. Commun.* 11 (1), 921. doi:10.1038/s41467-020-14591-8

Reimer, C., Caspani, L., Clerici, M., Ferrera, M., Kues, M., Peccianti, M., et al. (2014). Integrated frequency comb source of heralded single photons. *Opt. Express* 22 (6), 6535–6546. doi:10.1364/oe.22.006535

Reimer, C., Kues, M., Caspani, L., Wetzel, B., Roztocki, P., Clerici, M., et al. (2015). Cross-polarized photon-pair generation and bi-chromatically pumped optical parametric oscillation on a chip. *Nat. Commun.* 6 (1), 8236. doi:10.1038/ncomms9236

Reimer, C., Kues, M., Roztocki, P., Wetzel, B., Grazioso, F., Little, B. E., et al. (2016). Generation of multiphoton entangled quantum states by means of integrated frequency combs. *Science.* 351 (6278), 1176–1180. doi:10.1126/science.aad8532

Reimer, C., Sciara, S., Roztocki, P., Islam, M., Romero Corte´s, L., Zhang, Y., et al. (2019). High-dimensional one-way quantum processing implemented on d-level cluster states. *Nat. Phys.* 15 (2), 148–153. doi:10.1038/s41567-018-0347-x

Ribordy, G., Gautier, J.-D., Zbinden, H., and Gisin, N. (1998). Performance of InGaAs/InP avalanche photodiodes as gated-mode photon counters. *Appl. Opt.* 37 (12), 2272–2277. doi:10.1364/ao.37.002272

Rossi, A., Vallone, G., Chiuri, A., De Martini, F., and Mataloni, P. (2009). Multipath entanglement of two photons. *Phys. Rev. Lett.* 102 (15), 153902. doi:10.1103/physrevlett.102.153902

Rossi, A., Vallone, G., De Martini, F., and Mataloni, P. (2008). Generation of time-bin-entangled photons without temporal postselection. *Phys. Rev. A* 78 (1), 012345. doi:10.1103/physreva.78.012345

Roztocki, P., Kues, M., Reimer, C., Wetzel, B., Sciara, S., Zhang, Y., et al. (2017). Practical system for the generation of pulsed quantum frequency combs. *Opt. Express* 25 (16), 18940–18949. doi:10.1364/oe.25.018940

Roztocki, P., MacLellan, B., Islam, M., Reimer, C., Fischer, B., Sciara, S., et al. (2021). Arbitrary phase access for stable fiber interferometers. *Laser and Photonics Rev.* 15 (7), 2000524. doi:10.1002/lpor.202000524

Sangouard, N., Simon, C., De Riedmatten, H., and Gisin, N. (2011). Quantum repeaters based on atomic ensembles and linear optics. *Rev. Mod. Phys.* 83 (1), 33–80. doi:10.1103/revmodphys.83.33

Sansoni, L., Luo, K. H., Eigner, C., Ricken, R., Quiring, V., Herrmann, H., et al. (2017). A two-channel, spectrally degenerate polarization entangled source on chip. *npj Quantum Inf.* 3 (1), 5. doi:10.1038/s41534-016-0005-z

Santagiustina, F. B., Agnesi, C., Alarcón, A., Cabello, A., Xavier, G. B., Villoresi, P., et al. (2024). Experimental post-selection loophole-free time-bin and energy-time nonlocality with integrated photonics. *Optica* 11 (4), 498–511. doi:10.1364/optica.499247

Schaeff, C., Polster, R., Lapkiewicz, R., Fickler, R., Ramelow, S., and Zeilinger, A. (2012). Scalable fiber integrated source for higher-dimensional path-entangled photonic quNits. *Opt. Express* 20 (15), 16145–16153. doi:10.1364/oe.20.016145

Schlingemann, D., and Werner, R. F. (2001). Quantum error-correcting codes associated with graphs. *Phys. Rev. A* 65 (1), 012308. doi:10.1103/physreva.65.012308

Schreiber, A., Cassemiro, K. N., Potoček, V., Gábris, A., Mosley, P. J., Andersson, E., et al. (2010). Photons walking the line: a quantum walk with adjustable coin operations. *Phys. Rev. Lett.* 104 (5), 050502. doi:10.1103/physrevlett.104.050502

Sciara, S., Reimer, C., Kues, M., Roztocki, P., Cino, A., Moss, D. J., et al. (2019). Universal N-partite d-level pure-state entanglement witness based on realistic measurement settings. *Phys. Rev. Lett.* 122 (12), 120501. doi:10.1103/physrevlett.122.120501

Scott, R. E., Alsing, P. M., Smith, A. M., Fanto, M. L., Tison, C. C., Schneeloch, J., et al. (2019). Scalable controlled-not gate for linear optical quantum computing using microring resonators. *Phys. Rev. A* 100 (2), 022322. doi:10.1103/physreva.100.022322

Shadbolt, P. J., Verde, M. R., Peruzzo, A., Politi, A., Laing, A., Lobino, M., et al. (2012). Generating, manipulating and measuring entanglement and mixture with a reconfigurable photonic circuit. *Nat. Photonics* 6 (1), 45–49. doi:10.1038/nphoton.2011.283

Shams-Ansari, A., Renaud, D., Cheng, R., Shao, L., He, L., Zhu, D., et al. (2022). Electrically pumped laser transmitter integrated on thin-film lithium niobate. *Optica* 9 (4), 408–411. doi:10.1364/optica.448617

Sharping, J. E., Fiorentino, M., Coker, A., Kumar, P., and Windeler, R. S. (2001). Four-wave mixing in microstructure fiber. *Opt. Lett.* 26 (14), 1048–1050. doi:10.1364/ol.26.001048

Shen, S., Yuan, C., Zhang, Z., Yu, H., Zhang, R., Yang, C., et al. (2023). Hertz-rate metropolitan quantum teleportation. *Light Sci. and Appl.* 12 (1), 115. doi:10.1038/s41377-023-01158-7

Shin, D., Xu, F., Venkatraman, D., Lussana, R., Villa, F., Zappa, F., et al. (2016). Photon-efficient imaging with a single-photon camera. *Nat. Commun.* 7 (1), 12046. doi:10.1038/ncomms12046

Shor, P. W. (1994). "Algorithms for quantum computation: discrete logarithms and factoring," *Proceedings 35th annual symposium on foundations of computer science* (IEEE).

Shukla, V. K., and Ghosh, J. (2020). Generation of two different polarization-entangled biphoton states in a potassium titanyl phosphate waveguide device with multiple periodic poling. *Phys. Rev. A* 101 (2), 023832. doi:10.1103/physreva.101.023832

Silverstone, J. W., Santagati, R., Bonneau, D., Strain, M. J., Sorel, M., O'Brien, J. L., et al. (2015). Qubit entanglement between ring-resonator photon-pair sources on a silicon chip. *Nat. Commun.* 6 (1), 7948. doi:10.1038/ncomms8948

Sit, A., Bouchard, F., Fickler, R., Gagnon-Bischoff, J., Larocque, H., Heshami, K., et al. (2017). High-dimensional intracity quantum cryptography with structured photons. *Optica* 4 (9), 1006–1010. doi:10.1364/optica.4.001006

Slater, J. A., Branciard, C., Brunner, N., and Tittel, W. (2014). Device-dependent and device-independent quantum key distribution without a shared reference frame. *New J. Phys.* 16 (4), 043002. doi:10.1088/1367-2630/16/4/043002

Slussarenko, S., Weston, M. M., Chrzanowski, H. M., Shalm, L. K., Verma, V. B., Nam, S. W., et al. (2017). Unconditional violation of the shot-noise limit in photonic quantum metrology. *Nat. Photonics* 11 (11), 700–703. doi:10.1038/s41566-017-0011-5

Smith, B. J., Mahou, P., Cohen, O., Lundeen, J., and Walmsley, I. (2009). Photon pair generation in birefringent optical fibers. *Opt. Express* 17 (26), 23589–23602. doi:10.1364/oe.17.023589

Son, G., Han, S., Park, J., Kwon, K., and Yu, K. (2018). High-efficiency broadband light coupling between optical fibers and photonic integrated circuits. *Nanophotonics* 7 (12), 1845–1864. doi:10.1515/nanoph-2018-0075

Stucki, D., Zbinden, H., and Gisin, N. (2005). A Fabry–Perot-like two-photon interferometer for high-dimensional time-bin entanglement. *J. Mod. Opt.* 52 (18), 2637–2648. doi:10.1080/09500340500283821

Sultanov, V., Santiago-Cruz, T., and Chekhova, M. V. (2022). Flat-optics generation of broadband photon pairs with tunable polarization entanglement. *Opt. Lett.* 47 (15), 3872–3875. doi:10.1364/ol.458133

Sun, K., Wang, Y., Liu, Z.-H., Xu, X.-Y., Xu, J.-S., Li, C.-F., et al. (2020). Experimental quantum entanglement and teleportation by tuning remote spatial indistinguishability of independent photons. *Opt. Lett.* 45 (23), 6410–6413. doi:10.1364/ol.401735

Sun, P.-F., Yu, Y., An, Z.-Y., Li, J., Yang, C.-W., Bao, X.-H., et al. (2022). Deterministic time-bin entanglement between a single photon and an atomic ensemble. *Phys. Rev. Lett.* 128 (6), 060502. doi:10.1103/physrevlett.128.060502

Sun, Q.-C., Mao, Y.-L., Chen, S.-J., Zhang, W., Jiang, Y.-F., Zhang, Y.-B., et al. (2016). Quantum teleportation with independent sources and prior entanglement distribution over a network. *Nat. Photonics* 10 (10), 671–675. doi:10.1038/nphoton.2016.179

Taballione, C., van der Meer, R., Snijders, H. J., Hooijschuur, P., Epping, J. P., de Goede, M., et al. (2021). A universal fully reconfigurable 12-mode quantum photonic processor. *Mater. Quantum Technol.* 1 (3), 035002. doi:10.1088/2633-4356/ac168c

Taballione, C., Wolterink, T. A., Lugani, J., Eckstein, A., Bell, B. A., Grootjans, R., et al. (2019). 8× 8 reconfigurable quantum photonic processor based on silicon nitride waveguides. *Opt. Express* 27 (19), 26842–26857. doi:10.1364/oe.27.026842

Takenaka, H., Carrasco-Casado, A., Fujiwara, M., Kitamura, M., Sasaki, M., and Toyoshima, M. (2017). Satellite-to-ground quantum-limited communication using a 50-kg-class microsatellite. *Nat. Photonics* 11 (8), 502–508. doi:10.1038/nphoton.2017.107

Takesue, H., Fukuda, H., Tsuchizawa, T., Watanabe, T., Yamada, K., Tokura, Y., et al. (2008). Generation of polarization entangled photon pairs using silicon wire waveguide. *Opt. Express* 16 (8), 5721–5727. doi:10.1364/oe.16.005721

Takesue, H., and Inoue, K. (2004). Generation of polarization-entangled photon pairs and violation of Bell's inequality using spontaneous four-wave mixing in a fiber loop. *Phys. Rev. A* 70 (3), 031802. doi:10.1103/physreva.70.031802

Takesue, H., and Noguchi, Y. (2009). Implementation of quantum state tomography for time-bin entangled photon pairs. *Opt. Express* 17 (13), 10976–10989. doi:10.1364/oe.17.010976

Takesue, H., Tokura, Y., Fukuda, H., Tsuchizawa, T., Watanabe, T., Yamada, K., et al. (2007). Entanglement generation using silicon wire waveguide. *Appl. Phys. Lett.* 91 (20). doi:10.1063/1.2814040

Tanzilli, S., Tittel, W., De Riedmatten, H., Zbinden, H., Baldi, P., DeMicheli, M., et al. (2002). PPLN waveguide for quantum communication. *Eur. Phys. J. D - Atomic, Mol. Opt. Phys.* 18, 155–160. doi:10.1140/epjd/e20020019

Thew, R. T., Acin, A., Zbinden, H., and Gisin, N. (2003). Experimental realization of entangled qutrits for quantum communication. arXiv preprint quant-ph/0307122.

Thiel, H., Jehle, L., Chapman, R. J., Frick, S., Conradi, H., Kleinert, M., et al. (2024). Time-bin entanglement at telecom wavelengths from a hybrid photonic integrated circuit. *Sci. Rep.* 14 (1), 9990. doi:10.1038/s41598-024-60758-4

Tichy, M. C., Mintert, F., and Buchleitner, A. (2011). Essential entanglement for atomic and molecular physics. *J. Phys. B Atomic, Mol. Opt. Phys.* 44 (19), 192001. doi:10.1088/0953-4075/44/19/192001

Tittel, W., Brendel, J., Zbinden, H., and Gisin, N. (1998). Violation of Bell inequalities by photons more than 10 km apart. *Phys. Rev. Lett.* 81 (17), 3563–3566. doi:10.1103/physrevlett.81.3563

Tittel, W., Brendel, J., Zbinden, H., and Gisin, N. (2000). Quantum cryptography using entangled photons in energy-time Bell states. *Phys. Rev. Lett.* 84 (20), 4737–4740. doi:10.1103/physrevlett.84.4737

Toliver, P., Dailey, J. M., Agarwal, A., and Peters, N. A. (2015). Continuously active interferometer stabilization and control for time-bin entanglement distribution. *Opt. Express* 23 (4), 4135–4143. doi:10.1364/oe.23.004135

Torricelli, A., Contini, D., Pifferi, A., Caffini, M., Re, R., Zucchelli, L., et al. (2014). Time domain functional NIRS imaging for human brain mapping. *Neuroimage* 85, 28–50. doi:10.1016/j.neuroimage.2013.05.106

Tóth, G., and Gühne, O. (2005). Entanglement detection in the stabilizer formalism. *Phys. Rev. A* 72 (2), 022340. doi:10.1103/physreva.72.022340

Vagniluca, I., Da Lio, B., Rusca, D., Cozzolino, D., Ding, Y., Zbinden, H., et al. (2020). Efficient time-bin encoding for practical high-dimensional quantum key distribution. *Phys. Rev. Appl.* 14 (1), 014051. doi:10.1103/physrevapplied.14.014051

Valencia, A., Chekhova, M. V., Trifonov, A., and Shih, Y. (2002). Entangled two-photon wave packet in a dispersive medium. *Phys. Rev. Lett.* 88 (18), 183601. doi:10.1103/physrevlett.88.183601

Valivarthi, R., Puigibert, M. G., Zhou, Q., Aguilar, G. H., Verma, V. B., Marsili, F., et al. (2016). Quantum teleportation across a metropolitan fibre network. *Nat. Photonics* 10 (10), 676–680. doi:10.1038/nphoton.2016.180

Vallés, A., Hendrych, M., Svozilik, J., Machulka, R., Abolghasem, P., Kang, D., et al. (2013). Generation of polarization-entangled photon pairs in a Bragg reflection waveguide. *Opt. Express* 21 (9), 10841–10849. doi:10.1364/oe.21.010841

Vallone, G., Pomarico, E., De Martini, F., and Mataloni, P. (2008). One-way quantum computation with two-photon multiqubit cluster states. *Phys. Rev. A* 78 (4), 042335. doi:10.1103/physreva.78.042335

Varnava, M., Browne, D. E., and Rudolph, T. (2008). How good must single photon sources and detectors be for efficient linear optical quantum computation. *Phys. Rev. Lett.* 100 (6), 060502. doi:10.1103/physrevlett.100.060502

Vedovato, F., Agnesi, C., Tomasin, M., Avesani, M., Larsson, J. Å., Vallone, G., et al. (2018). Postselection-loophole-free Bell violation with genuine time-bin entanglement. *Phys. Rev. Lett.* 121 (19), 190401. doi:10.1103/physrevlett.121.190401

Vernon, Z., Menotti, M., Tison, C., Steidle, J., Fanto, M., Thomas, P., et al. (2017). Truly unentangled photon pairs without spectral filtering. *Opt. Lett.* 42 (18), 3638–3641. doi:10.1364/ol.42.003638

Walmsley, I. (2015). Quantum optics: science and technology in a new light. *Science* 348 (6234), 525–530. doi:10.1126/science.aab0097

Walther, P., Aspelmeyer, M., Resch, K. J., and Zeilinger, A. (2005b). Experimental violation of a cluster state Bell inequality. *Phys. Rev. Lett.* 95 (2), 020403. doi:10.1103/physrevlett.95.020403

Walther, P., Resch, K. J., Rudolph, T., Schenck, E., Weinfurter, H., Vedral, V., et al. (2005a). Experimental one-way quantum computing. *Nature* 434 (7030), 169–176. doi:10.1038/nature03347

Wang, J., Paesani, S., Ding, Y., Santagati, R., Skrzypczyk, P., Salavrakos, A., et al. (2018). Multidimensional quantum entanglement with large-scale integrated optics. *Science.* 360 (6386), 285–291. doi:10.1126/science.aar7053

Wang, J.-Y., Yang, B., Liao, S.-K., Zhang, L., Shen, Q., Hu, X.-F., et al. (2013). Direct and full-scale experimental verifications towards ground–satellite quantum key distribution. *Nat. Photonics* 7 (5), 387–393. doi:10.1038/nphoton.2013.89

Wang, L., Hong, C., and Friberg, S. (2001). Generation of correlated photons via four-wave mixing in optical fibres. *J. Opt. B Quantum semiclassical Opt.* 3 (5), 346–352. doi:10.1088/1464-4266/3/5/311

Wang, M., and Yan, F. (2016). Quantum teleportation of a generic two-photon state with weak cross-Kerr nonlinearities. *Quantum Inf. Process.* 15, 3383–3392. doi:10.1007/s11128-016-1341-9

Wang, Y., Hu, Z., Sanders, B. C., and Kais, S. (2020). Qudits and high-dimensional quantum computing. *Front. Phys.* 8, 589504. doi:10.3389/fphy.2020.589504

Wilmart, Q., Brision, S., Hartmann, J.-M., Myko, A., Ribaud, K., Petit-Etienne, C., et al. (2021). A complete Si photonics platform embedding ultra-low loss waveguides for O-and C-band. *J. Light. Technol.* 39 (2), 532–538. doi:10.1109/jlt.2020.3030123

Wilmart, Q., El Dirani, H., Tyler, N., Fowler, D., Malhouitre, S., Garcia, S., et al. (2019). A versatile silicon-silicon nitride photonics platform for enhanced functionalities and applications. *Appl. Sci.* 9 (2), 255. doi:10.3390/app9020255

Wilmart, Q., Guerber, S., Faugier-Tovar, J., Ibrahimi, Y., Petit-Etienne, C., Youssef, L., et al. (2022). "A device library for the ultra-low loss Si3N4 platform,"Q. Wilmart, S. Guerber, J. Faugier-Tovar, Y. Ibrahimi, C. Petit-Etienne, and L. Youssef, XVII, 33. doi:10.1117/12.2606853*Silicon Photonics XVII*

Wootters, W. K., and Zurek, W. H. (1982). A single quantum cannot be cloned. *Nature* 299 (5886), 802–803. doi:10.1038/299802a0

Xiong, C., Zhang, X., Mahendra, A., He, J., Choi, D.-Y., Chae, C., et al. (2015). Compact and reconfigurable silicon nitride time-bin entanglement circuit. *Optica* 2 (8), 724–727. doi:10.1364/optica.2.000724

Yao, Z., Wu, K., Tan, B. X., Wang, J., Li, Y., Zhang, Y., et al. (2018). Integrated silicon photonic microresonators: emerging technologies. *IEEE J. Sel. Top. Quantum Electron.* 24 (6), 1–24. doi:10.1109/jstqe.2018.2846047

Ye, Z., Zhao, P., Karlsson, M., and Andrekson, P. A. (2022). "Ultralow-loss silicon nitride waveguides for parametric amplification," In *Optical Fiber Communication Conference.* Optica Publishing Group, W4J-3.

Yin, J., Cao, Y., Li, Y.-H., Liao, S.-K., Zhang, L., Ren, J.-G., et al. (2017). Satellite-based entanglement distribution over 1200 kilometers. *Science* 356 (6343), 1140–1144. doi:10.1126/science.aan3211

Yin, J., Ren, J.-G., Lu, H., Cao, Y., Yong, H.-L., Wu, Y.-P., et al. (2012). Quantum teleportation and entanglement distribution over 100-kilometre free-space channels. *Nature* 488 (7410), 185–188. doi:10.1038/nature11332

Yu, H., Govorov, A. O., Song, H.-Z., and Wang, Z. (2024). Time-encoded photonic quantum states: generation, processing, and applications. *Appl. Phys. Rev.* 11 (4). doi:10.1063/5.0232085

Yu, H., Sciara, S., Chemnitz, M., Montaut, N., Crockett, B., Fischer, B., et al. (2025). Quantum key distribution implemented with d-level time-bin entangled photons. *Nat. Commun.* 16, 171. doi:10.1038/s41467-024-55345-0

Yu, L., Natarajan, C. M., Horikiri, T., Langrock, C., Pelc, J. S., Tanner, M. G., et al. (2015). Two-photon interference at telecom wavelengths for time-bin-encoded single photons from quantum-dot spin qubits. *Nat. Commun.* 6 (1), 8955. doi:10.1038/ncomms9955

Zbinden, H., Brendel, J., Gisin, N., and Tittel, W. (2001). Experimental test of nonlocal quantum correlation in relativistic configurations. *Phys. Rev. A* 63 (2), 022111. doi:10.1103/physreva.63.022111

Zeilinger, A., Horne, M. A., Weinfurter, H., and Żukowski, M. (1997). Three-particle entanglements from two entangled pairs. *Phys. Rev. Lett.* 78 (16), 3031–3034. doi:10.1103/physrevlett.78.3031

Zeng, H., He, Z.-Q., Fan, Y.-R., Luo, Y., Lyu, C., Wu, J.-P., et al. (2024). Quantum light generation based on GaN microring toward fully on-chip source. *Phys. Rev. Lett.* 132 (13), 133603. doi:10.1103/physrevlett.132.133603

Zhang, H., Zhang, C., Hu, X.-M., Liu, B.-H., Huang, Y.-F., Li, C.-F., et al. (2019). Arbitrary two-particle high-dimensional Bell-state measurement by auxiliary entanglement. *Phys. Rev. A* 99 (5), 052301. doi:10.1103/physreva.99.052301

Zhang, J., Itzler, M. A., Zbinden, H., and Pan, J.-W. (2015). Advances in InGaAs/InP single-photon detector systems for quantum communication. *Light Sci. and Appl.* 4 (5), e286–e. doi:10.1038/lsa.2015.59

Zhang, L., Cui, C., and Fan, L. (2022). "On-chip reconfigurable entangled photon-pair sources for quantum parallel processing." In *CLEO: QELS_fundamental science*, Optica Publishing Group, FM5C-3.

Zhang, Q., Langrock, C., Takesue, H., Xie, X., Fejer, M., and Yamamoto, Y. (2008). Generation of 10-GHz clock sequential time-bin entanglement. *Opt. Express* 16 (5), 3293–3298. doi:10.1364/oe.16.003293

Zhang, Q., Wu, K., and Poon, A. W. (2024). Polarization entanglement generation in silicon nitride waveguide-coupled dual microring resonators. *Opt. Express* 32 (13), 22804–22816. doi:10.1364/oe.518985

Zhang, X., Bell, B. A., Mahendra, A., Xiong, C., Leong, P. H., and Eggleton, B. J. (2018). Integrated silicon nitride time-bin entanglement circuits. *Opt. Lett.* 43 (15), 3469–3472. doi:10.1364/ol.43.003469

Zhang, Z., Yuan, C., Shen, S., Yu, H., Zhang, R., Wang, H., et al. (2021). High-performance quantum entanglement generation via cascaded second-order nonlinear processes. *npj Quantum Inf.* 7 (1), 123. doi:10.1038/s41534-021-00462-7

Zhou, D., Zeng, B., Xu, Z., and Sun, C. (2003). Quantum computation based on d-level cluster state. *Phys. Rev. A* 68 (6), 062303. doi:10.1103/physreva.68.062303

Zhu, E. Y., Tang, Z., Qian, L., Helt, L. G., Liscidini, M., Sipe, J., et al. (2012). Direct generation of polarization-entangled photon pairs in a poled fiber. *Phys. Rev. Lett.* 108 (21), 213902. doi:10.1103/physrevlett.108.213902

Zhu, P., Liu, Y., Wu, C., Xue, S., Yu, X., Zheng, Q., et al. (2020). Near 100% spectral-purity photons from reconfigurable micro-rings. *Chin. Phys. B* 29 (11), 114201. doi:10.1088/1674-1056/abbb28